

Bernini: Latent Semantic Planning for Video Diffusion

Bernini Team, Bytedance

Abstract

Multimodal large language models (MLLMs) and diffusion models have each reached remarkable maturity: MLLMs excel at reasoning over heterogeneous multimodal inputs with strong semantic grounding, while diffusion models synthesize images and videos with photorealistic fidelity. We argue that these two families can be unified through a simple division of labor: MLLMs perform semantic planning, while diffusion models render pixels from high-level semantic guidance and low-level visual features. Building on this idea, we propose **Bernini**, a unified framework for video generation and editing. An MLLM-based **planner** predicts the target semantic representation directly in the ViT embedding space, and a DiT-based **renderer** synthesizes pixels conditioned on this plan, augmented by text features and, for editing, source VAE features for detail preservation. Because semantics serve as the interface, the planner and renderer can be trained separately and only lightly co-trained, preserving the pretrained strengths of both components while keeping training efficient. To better handle multiple visual inputs, we introduce Segment-Aware 3D Rotary Positional Embedding (SA-3D RoPE), and further incorporate chain-of-thought reasoning in the planner to better transfer understanding into generation. Bernini achieves state-of-the-art performance across a wide range of video generation and editing benchmarks, with the MLLM’s pretrained understanding translating into strong generalization on challenging editing tasks.

Date: May 22, 2026

Correspondence: zhyuan001@gmail.com

Project Page: <https://bernini-ai.github.io>

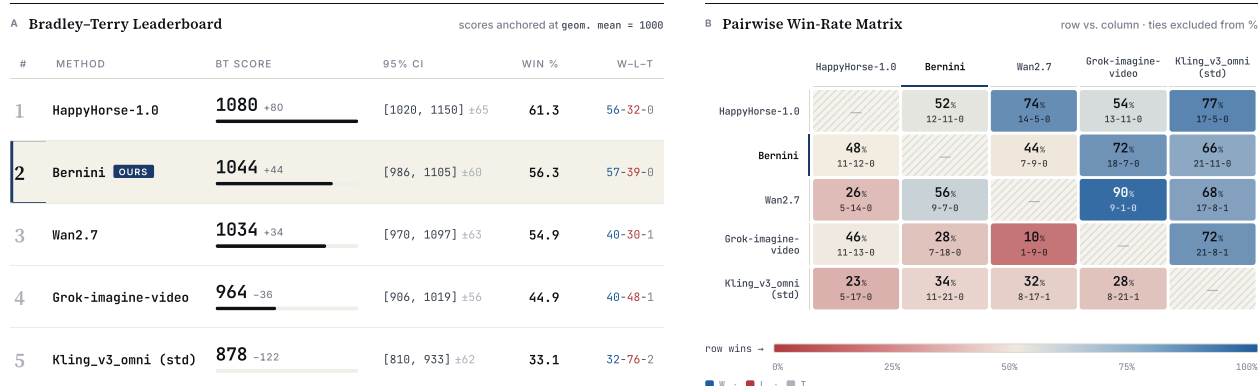


Figure 1 Video editing leaderboard. Pairwise human preferences on open-ended video editing (no restriction on instruction type). **(A) Leaderboard.** BT scores [5] with 95% bootstrap CIs; **Win %** = $1/(1 + 10^{-(s-1000)/400})$ vs. avg. opponent; **W-L-T** raw record. **(B) Win-rate matrix.** $W/(W+L)$; Bernini: 480p/24 fps; baselines: 720p/24 fps.



Figure 2 Bernini supports diverse video generation tasks within a unified framework, including text-to-video (T2V), subject-to-video (R2V), video editing (V2V), and reference-guided video editing (RV2V).

Contents

1	Introduction	4
2	Methods	5
2.1	Architecture	5
2.1.1	MLLM-based Planner	5
2.1.2	DiT-based Renderer	6
2.2	Training Objectives	6
3	Data	7
3.1	Pre-training Data	7
3.2	Diverse Image Editing and Image-to-Video Editing Data	9
3.3	High-quality Video-to-Video Editing Data	9
3.4	Reference-image-guided Video Generation and Editing Data	11
3.5	Reference-video-guided Video Generation Data	11
3.6	Reasoning-augmented Video Data	12
4	Training and Inference	13
4.1	Training Pipelines	14
4.2	Inference Strategy	16
5	Infrastructure	17
5.1	Training Infrastructure	17
5.2	Inference Parallelism	18
5.3	Model Distillation	18
6	Experiments	18
6.1	Implementation Details	18
6.2	Bernini-Bench	18
6.3	Video Editing	20
6.4	Reasoning-augmented Video Editing	22
6.5	Video Generation	23
6.6	Ablation Studies	24
6.7	Generalizations	25
7	Related Work	25
8	Conclusion and Limitations	26
9	Contributions and Acknowledgements	27
A	MLLM Prompts for Bernini-Bench Evaluation	34
B	Experimental Results	39
B.1	More Qualitative Comparison with SoTA Methods	39
B.2	Qualitative Comparison of Video Editing with Reasoning	40
B.3	More Generalization Results	40

1 Introduction

Multimodal large language models (MLLMs) [11, 44, 69] and diffusion models [20, 36, 53, 60, 70] have matured along largely independent trajectories. Modern MLLMs read long instructions, reason over multiple reference images, and ground their answers in a complex multimodal context. Diffusion models, meanwhile, have become the default tool for photorealistic image and video synthesis at high resolutions and long durations. The natural next step is to combine these two mature families into a single system that both understands intent and generates the desired output, supporting unified understanding, generation, and editing within one model. However, how to do so effectively remains an open question.

Our approach begins with two simple observations. First, MLLMs are naturally suited to semantic reasoning: interpreting long instructions, grounding on multiple references, and forming an internal representation of what the output should be. Second, diffusion generation decomposes cleanly into semantic guidance and detail preservation. The high-level content is determined by a compact semantic signal, while fine-grained fidelity, and in editing also consistency with the source input, requires dense pixel-level latents such as VAE features. Crucially, the semantic signal itself need not be high-resolution to be effective. A handful of semantic tokens are enough to specify an entire scene.

These observations suggest a clean division of labor: let the MLLM carry out semantic reasoning, and let the diffusion model focus on synthesis, using semantic features as its primary condition and pixel-level features only where detail preservation demands them. A natural question is what representation should carry the semantic signal between the two. We anchor this interface to a representation that already exists within MLLM itself, namely its own ViT embedding space [19, 58, 71]. The MLLM already reasons and represents visual content in this space, so training it to plan the target in ViT embeddings aligns naturally with its pretrained representations and requires minimal adaptation.

We instantiate this principle as **Bernini**, a unified framework for multimodal understanding, generation, and editing. Bernini consists of a **planner**, based on an MLLM, that predicts the target’s visual representation in the continuous ViT embedding space. Following a masked generative modeling paradigm [39], a lightweight ViT embedding decoder on top of the MLLM recovers randomly masked target ViT tokens from the hidden states of the MLLM, and at inference progressively fills in the full target representation from fully masked tokens. The **renderer**, a Diffusion Transformer (DiT) [55], then synthesizes the final image or video through flow-matching [43] denoising over VAE latent tokens, conditioned on the semantic embedding from the planner through cross-attention and augmented with text features. For editing tasks, VAE features of the source input are additionally injected to preserve detail and consistency.

To unify different task types, we adopt a shared input protocol across text-to-video, subject-to-video, and editing, achieving broad modality coverage without task-specific architectures. For multiple visual sources within a unified sequence, we further introduce **Segment-Aware 3D Rotary Positional Embedding (SA-3D RoPE)**, which augments standard spatiotemporal rotary embeddings [64] with a segment-index-conditioned phase modulation. Finally, to amplify the contribution of understanding to generation, the planner is equipped with a **Chain-of-Thought (CoT) mechanism** [28, 77] that performs reasoning in latent space before producing the final embedding. Because semantics serve as the interface, the two components can be trained largely independently and only lightly co-trained thereafter, preserving the MLLM’s pretrained capabilities and allowing its multimodal understanding to transfer directly into diverse downstream generation tasks. Our contributions are summarized as follows:

- We propose **Bernini**, a unified framework for generation, and editing that uses the MLLM’s own ViT embedding space as a semantic bridge to the diffusion generator, allowing pretrained understanding to transfer directly into generation and enabling strong generalization across diverse video tasks.
- We design a suite of data construction pipelines that yield a large-scale, multi-task corpus for unified video generation and editing, spanning video- and image-pair pretraining data, high-quality propagation-based and motion-aware video editing data, and reference-image- and reference-video-guided generation data, providing the diverse and high-fidelity supervision required to train Bernini across all tasks.
- Bernini achieves state-of-the-art performance across a wide range of video generation, editing, and subject-to-video benchmarks, including OpenVE-Bench, OpenS2V-Eval, and our newly proposed Bernini-Bench.

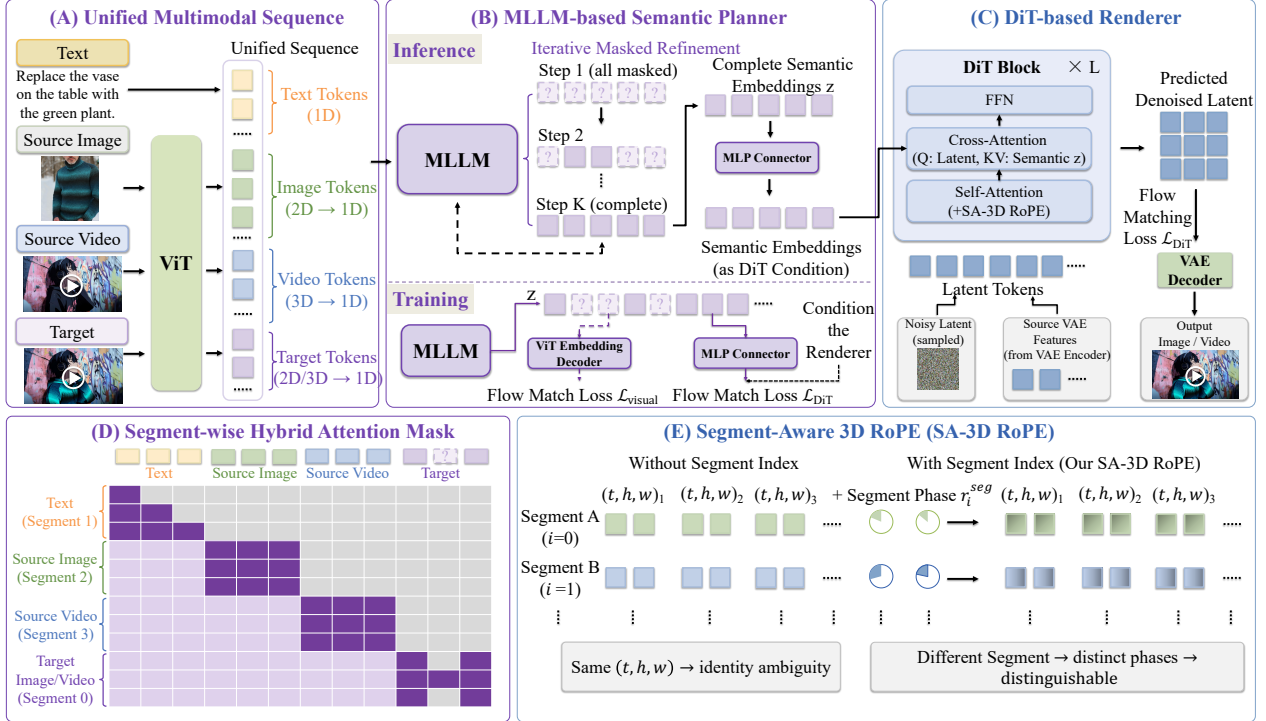


Figure 3 Overview of Bernini. (A) Visual and text inputs are serialized into a unified 1D sequence. (B) The MLLM planner predicts target semantic embeddings from masked targets and conditions the renderer. (C) The DiT-based renderer performs flow matching in the VAE latent space conditioned on semantic embeddings and source VAE features. (D) Bernini uses a segment-wise hybrid attention mask in MLLM. (E) Segment-aware 3D RoPE disambiguates visual tokens from different segments.

2 Methods

2.1 Architecture

As illustrated in Fig. 3, Bernini consists of two main components: an MLLM-based planner and a DiT-based renderer. Taking multimodal conditions as input, the MLLM performs multimodal understanding and semantic reasoning to produce the desired target content. An MLP connector then maps these hidden states into the conditioning representation required by the DiT-based renderer. Conditioned on these semantic features, together with additional text features and source visual conditions when available, the DiT-based renderer synthesizes the final image or video in the VAE latent space.

2.1.1 MLLM-based Planner

Unified Input Formulation. To support diverse tasks within a single framework, Bernini adopts a unified multimodal input formulation. All task instances, including text-to-video generation, text-to-image generation, subject-to-video generation, and image or video editing, are serialized into a shared token sequence composed of textual tokens and visual tokens from the source inputs and the target output. Formally, given a multimodal input sequence, the MLLM encodes the entire sequence and produces contextualized hidden states \mathbf{z} that capture the target intent conditioned on the input context:

$$\mathbf{z} = \text{MLLM}(\mathbf{t}, \mathbf{v}_1^{\text{src}}, \mathbf{v}_2^{\text{src}}, \dots, \mathbf{v}_N^{\text{src}}, \mathbf{v}^{\text{tgt}}) \quad (1)$$

where \mathbf{t} denotes the input textual embeddings, $\mathbf{v}_i^{\text{src}}$ denotes the ViT embeddings of the i -th source visual input, N is the number of source inputs, and \mathbf{v}^{tgt} denotes the visual embeddings corresponding to the target output. During training, \mathbf{v}^{tgt} is partially masked at random, while during inference it is initialized as fully masked.

Mask-based Semantic Planning. Motivated by the intrinsically bidirectional nature of visual semantic latents, a masked generative modeling paradigm [8, 27] is adopted to better capture contextual dependencies. To mitigate the visual information loss introduced by discrete tokenization, we represent visual tokens as dense embeddings, which serve as both the input and output of the MLLM.

During training, a subset of target visual tokens is randomly masked and replaced with a shared mask token. The masking ratio is sampled from a Beta distribution, $r \sim \text{Beta}(\alpha, \beta)$, where α and β are hyperparameters. The MLLM is then trained to infer the masked content from the remaining visible tokens together with the surrounding multimodal context. The resulting hidden states serve as semantic embeddings for the target visual content. To recover the target ViT embeddings from these semantic embeddings, we follow the design philosophy of MAR [39]. Specifically, the hidden states at masked positions are fed into the ViT embedding Decoder, which consists of an MLP followed by a ResNet-based prediction head. The decoder predicts the corresponding ground-truth ViT embeddings and is trained with a flow-matching objective in the ViT embedding space.

During inference, all target visual tokens are initialized as masked tokens. The MLLM then progressively decodes the target representation over K refinement steps, following the standard masked generative paradigm. At step k , the mask ratio is scheduled as $\text{mask_ratio}(k, K) = \cos\left(\frac{\pi}{2} \cdot \frac{k+1}{K}\right)$, so that the number of masked tokens gradually decreases over time. At each step, the currently predicted tokens are fed back into the MLLM and used as partial observations for the next round of prediction. This iterative process progressively refines the target representation from coarse to fine, until a complete target ViT embedding sequence is obtained.

2.1.2 DiT-based Renderer

The DiT-based renderer performs diffusion in the VAE latent space, using the contextualized hidden states \mathbf{z} from the MLLM in Eq. 1 as conditioning features, and decodes the resulting target latent into the final output. In addition, VAE features extracted from the source image or video are incorporated to preserve low-level details and ensure consistency with the source content.

Segment-Aware 3D RoPE. In DiTs, 3D RoPE is commonly used to encode temporal and spatial positions for visual tokens. It encodes the temporal, vertical, and horizontal positions of each visual token into three rotary subspaces and concatenates them to form $\mathbf{r}_{t,h,w}$. When Bernini concatenates all visual inputs and output as a unified sequence, tokens from different segments (different reference images, source videos, or target output) may share the same (t, h, w) coordinates, making it difficult to distinguish different identities. To address this issue, SA-3D RoPE is introduced, which assigns each visual segment an index i , e.g. $i = 0$ for the target segment and $i = 1, 2, \dots$ for input segments, and incorporates the segment index directly into the rotary position encoding. To be specific, a full-dimensional rotary frequency vector $\mathbf{r}_i^{\text{seg}}$ is constructed to additionally encode the segment index i for each segment index. Then, SA-3D RoPE can be calculated through

$$\tilde{\mathbf{r}}_{t,h,w,i} = \mathbf{r}_{t,h,w} \odot \mathbf{r}_i^{\text{seg}}, \quad (2)$$

where \odot denotes multiplication of complexes in element order. This introduces a segment-dependent global phase modulation on top of the original spatiotemporal phase, allowing attention to distinguish tokens from different segments while preserving the original spatial-temporal modeling properties of 3D RoPE.

2.2 Training Objectives

During training, the MLLM is optimized with the standard next-token prediction (NTP) loss \mathcal{L}_{ntp} to preserve its multimodal understanding capability. The ViT embedding decoder and the DiT renderer are both trained with standard flow-matching objectives, denoted as $\mathcal{L}_{\text{visual}}$ and \mathcal{L}_{dit} in the continuous ViT embedding space and the VAE latent space, respectively. The two objectives share the same formulation, differing only in the definition of the target representation and the corresponding velocity field. The overall training objective is the weighted sum of these three losses:

$$\mathcal{L} = \lambda_{\text{text}}\mathcal{L}_{\text{ntp}} + \lambda_{\text{visual}}\mathcal{L}_{\text{visual}} + \lambda_{\text{dit}}\mathcal{L}_{\text{dit}}, \quad (3)$$

where λ_{text} , λ_{visual} , and λ_{dit} are the corresponding loss weights.

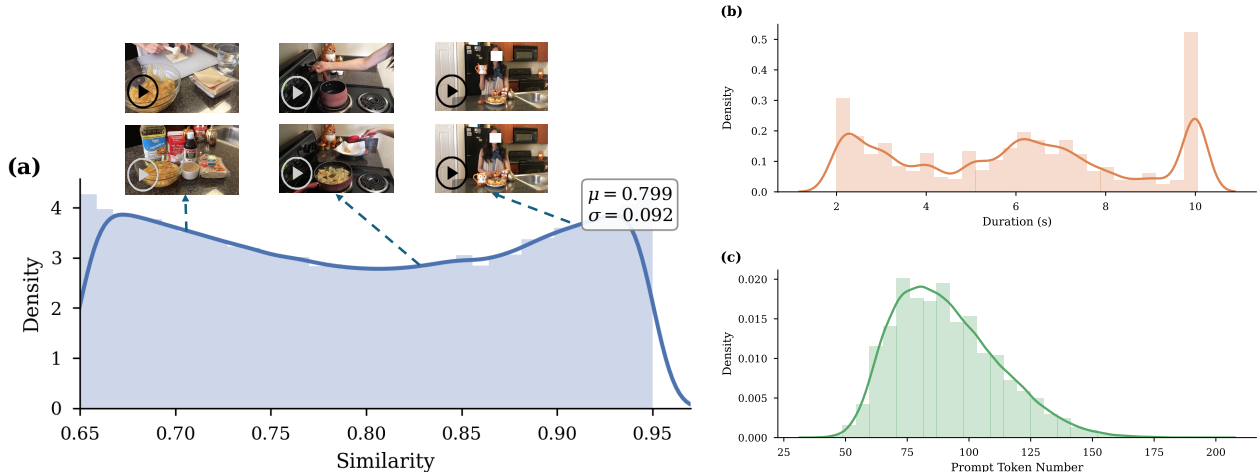


Figure 4 Dataset statistics of the collected video pairs. (a) Similarity score distribution between 0.65 and 0.95, with representative video pairs, extracted from the same raw video, visualized at their corresponding scores. (b) Distribution of video durations. (c) Distribution of prompt token counts.

3 Data

Bernini is trained in a diverse corpus that includes text-only, multimodal understanding, image/video generation, and image/video editing tasks. Although substantial progress has been made in constructing understanding data [78, 95], image editing data [10, 35, 74, 75, 88, 90, 93, 96], and a limited amount of video editing data [2, 48, 99] has also been explored, the current landscape remains insufficient for training general-purpose video editing models. Video editing spans diverse task types, yet mature and scalable data construction pipelines are still lacking. In addition to incorporating existing open-source data into our training corpus, we further explore a series of data construction strategies for both large-scale pretraining and high-quality supervised fine-tuning, including video-to-video editing, reference-image-based video generation and editing, reference-video-based video generation, and reasoning-augmented video data.

3.1 Pre-training Data

Video-pair Data. Current video editing models are constrained by the limited scale and quality of available training data, as existing video editing datasets are often noisy and rely on immature construction pipelines. This challenge makes large-scale video-pair pre-training essential. To this end, we constructed a large-scale dataset comprising 20 million video pairs from general T2V corpora. Our pipeline constructs diverse and balanced video pairs from raw videos through similarity-based filtering, content-aware sampling, and coarse-to-fine instruction generation.

Specifically, for video clips originating from the same raw video, we compute their global representations using X-CLIP [50] and compute pairwise similarity scores between video pairs. The selected video pairs that jointly satisfy the following conditions: (1) a similarity score between 0.65 and 0.95; (2) a duration between 2 and 10 seconds; (3) a 1:1 ratio of human-centric to non-human-centric content, which is annotated by Qwen3-VL-30B-A3B-Instruct [4]; and (4) limiting each raw video to a maximum of 100 pairs. This approach ensures a balance between spatio-temporal coherence and content variety. Finally, to generate high-quality instructional prompts, we employ Qwen3-VL-235B-A22B-Instruct [4] using a coarse-to-fine strategy. This approach first generates a coarse transition description between the video clips, which is subsequently refined into a detailed prompt. This enables fine-grained descriptions of camera motion as well as changes in the foreground and background.

Figure 4 presents the statistical distributions of our collected video pairs, including similarity scores, video durations, and generated prompt token counts. The similarity scores are approximately uniformly distributed, while the video durations and prompt lengths span a wide spectrum, demonstrating the overall diversity of



Figure 5 Examples of video pairs extracted from general T2V corpora, along with their generated dense prompts.

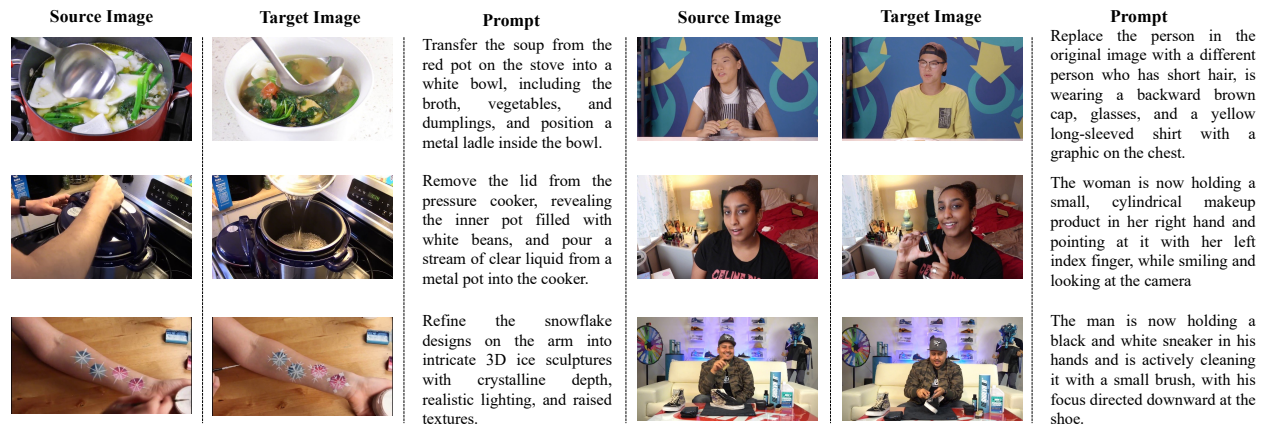


Figure 6 Examples of image pairs extracted from videos, along with their corresponding generated prompts.

our dataset. Furthermore, Fig. 5 shows examples of the constructed video pairs alongside their corresponding generated dense prompts. Each prompt is structured to first detail the camera motion, followed by descriptions of the foreground and background changes.

Image-pair Data. Similarly, a large-scale image manipulation dataset comprising nearly 30 million image pairs is constructed from tutorial videos [52]. These videos capture naturally occurring and often complex visual transformations, providing diverse and realistic variations that help establish strong semantic alignment between image pairs. The construction pipeline is described below. Key frames are sampled from over 300k videos, while low-motion or scaling-dominated frames are filtered based on inter-frame transformations, and blur detection is further applied to remove low-quality frames. For each video, image pairs are formed from the extracted frames, and pairwise similarities are computed using CLIP embeddings [58]. Pairs with similarity scores within a predefined range, i.e., [0.75, 0.95], are retained to exclude both near-duplicate and semantically unrelated pairs. Finally, Qwen3-VL-30B-A3B-Instruct [4] is used to generate textual prompts describing the visual differences between selected image pairs. Figure 6 shows examples of the constructed image pairs.

Interleaved Image-text Data. Inspired by prior work [13, 15], both web and video data are leveraged as key sources for constructing interleaved image-text data. For web data, following [15], around 10 million interleaved samples are first built from OmniCorpus [38]. Beyond the basic filtering in [15], Qwen3-32B [84] is used to regenerate the textual content, improving fluency and coherence, and subject-aware question-answer

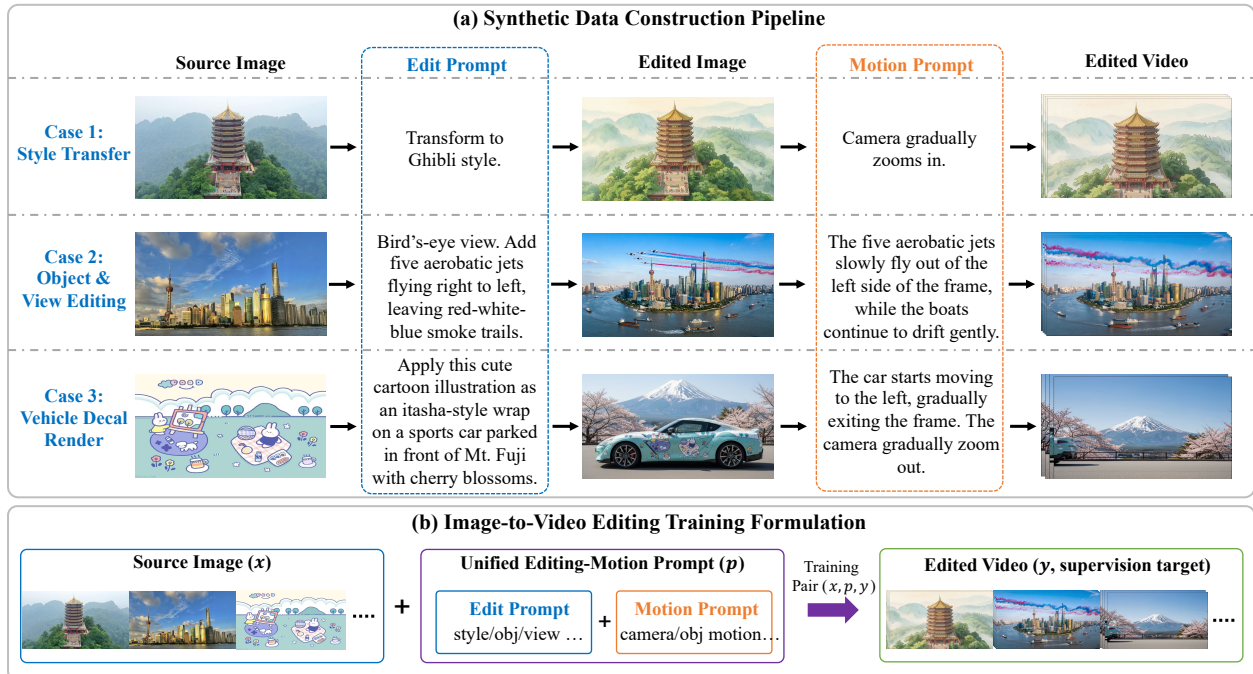


Figure 7 Example of generated Image Editing and Image-to-Video Editing Data.

pairs are further introduced for augmentation. For video data, up to 8 key frames are extracted from each video in the general T2V corpus, and Qwen3-VL-30B-A3B-Instruct [4] is employed to generate textual transitions between frames, yielding 2 million additional video-derived samples.

3.2 Diverse Image Editing and Image-to-Video Editing Data

Compared with image editing, constructing high-quality and diverse video-to-video editing data at scale remains significantly more difficult. Meanwhile, image-to-image editing has benefited from much more mature models and data resources. This suggests a practical route for improving video editing: reformulating part of the video editing problem as image-to-video editing, such that image-level editing capability can be transferred to video generation and eventually benefit video-to-video editing. In this way, image editing data serves not only as an auxiliary source of supervision, but also as a means to enrich the diversity and effectiveness of video editing training. Diverse image editing prompts are constructed through two complementary mechanisms. The first starts from a large pool of real-world user instructions, from which multiple candidate prompts are sampled for each source image; an MLLM then selects the most suitable candidate and rewrites it into the final editing prompt. The second maintains a dynamic editing prompt bank to encourage diversity. Conditioned on the source image and the current prompt bank, the MLLM generates a new editing instruction with high semantic distinctiveness. Editing prompt with high novelty are inserted into the bank, while less diverse ones are discarded once the bank reaches its capacity. After edited images are obtained, corresponding motion prompts are further generated by the MLLM to synthesize target videos. This process yields two types of training data: image editing triplets (Source Image, Edited Image, Edit Prompt), and image-to-video triplets (Source Image, Video, Edit Prompt+Motion Prompt). These data provide diverse supervision for transferring image editing knowledge to video editing. Examples can be found in Fig. 7.

3.3 High-quality Video-to-Video Editing Data

Propagation-based Data Boosting. We first construct initial addition and removal data with DiffuEraser [40] and replacement data with VACE [31], but these data suffer from artifacts and limited edit diversity. For instance, the removal data contains visible artifacts, while the replacement samples are constrained to generating objects with shapes consistent with the originals, which can degrade model performance. To

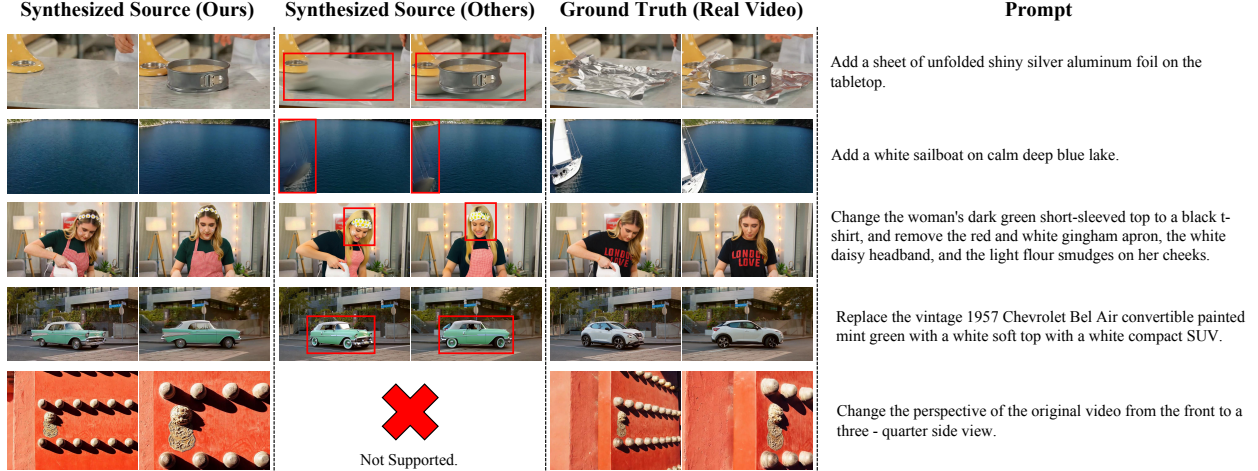


Figure 8 Examples of generated propagation-based edit data. Compared with existing methods, our method yields higher-quality results. Diffuserasr [40] (Rows 1-2) introduces obvious visual artifacts, while VACE [31] (Rows 3-4) suffers from character inconsistency and unnatural identical vehicle shape. Furthermore, our method enables more editing tasks (Row 5) that are unattainable by previous works.

address these issues, we first train a base propagation model on the initial editing data mentioned above, where the model takes a source video, an edited first frame, and an editing prompt as input to generate the target edited video. We then combine this propagation model with a strong image editing model to build high-quality video editing data for common tasks such as addition, removal, replacement, and style transfer. Benefiting from the high quality of the edited first frames produced by the image editing model, the resulting edited videos also exhibit strong visual quality. To further improve the quality of data, we swap the source and edited video pairs and regenerate matching prompts with the MLLM for addition, removal and replacement tasks. Examples can be found in Fig. 8.

Human Motion-aware Data. A strong video editing model should not only edit the target region accurately, but also adapt the surrounding scene to the consequences of the edit, especially in human-object interaction scenarios where object changes may naturally alter human pose and motion. However, such motion-aware editing data is difficult to collect and is poorly covered by existing synthesis pipelines. To address this, we propose a dual-branch data synthesis framework that combines the complementary strengths of image-to-video (I2V) generation and video-to-video (V2V) editing. Given an edited first frame and the source video, the I2V branch introduces motion adaptation, while the V2V branch preserves source motion consistency. Their outputs are fused with weighted guidance, enabling a controllable trade-off between motion preservation and action adaptation.

Let V denotes the source video, I the edited first frame, and T_{I2V} and T_{V2V} the prompts used in the two branches. We define

$$\begin{aligned}
 \hat{\epsilon} = & \alpha(w_{Full}^{I2V} \cdot \epsilon(T_{I2V}, \emptyset, I) - w_T^{I2V} \cdot \epsilon(\emptyset, \emptyset, I) - w_I^{I2V} \cdot \epsilon(T_{I2V}, \emptyset, \emptyset)) \\
 & + \beta(w_{Full}^{V2V} \cdot \epsilon(T_{V2V}, V, \emptyset) - w_T^{V2V} \cdot \epsilon(\emptyset, V, \emptyset) - w_V^{V2V} \cdot \epsilon(T_{V2V}, \emptyset, \emptyset)) \\
 \text{s.t. } & w_{Full}^{I2V} - w_T^{I2V} - w_I^{I2V} = 1, \quad w_{Full}^{V2V} - w_T^{V2V} - w_V^{V2V} = 1, \quad \alpha + \beta = 1
 \end{aligned} \tag{4}$$

Here, w_{Full}^{I2V} , w_T^{I2V} , and w_I^{I2V} are the classifier-free guidance weights for the full, text-dropped, and image-dropped conditions in the I2V branch, respectively. w_{Full}^{V2V} , w_T^{V2V} , and w_V^{V2V} are defined analogously for the V2V branch. The coefficients α and β control the contributions of the two branches. This formulation allows the I2V branch to emphasize action adaptation while the V2V branch preserves source motion consistency. Examples of motion-aware editing data generated by this method are shown in Fig. 9.



Figure 9 Examples of generated motion-aware editing data. Our approach successfully synthesizes natural motions while maintaining consistency with the source videos. Specifically, it rationalizes human motions after object replacement and removal (Rows 1-2), and rationalizes interactive motions after adding a person (Row 3).

3.4 Reference-image-guided Video Generation and Editing Data

We construct training data for two tasks: reference-to-video (R2V) and reference+video-to-video (RV2V). R2V data spans two domains, general objects and persons, each requiring a tailored pipeline. RV2V data is then synthesized on top of R2V via instruction-based video editing.

General-object R2V. For each source video, we sample keyframes and prompt an MLLM to identify the 3 to 5 most salient objects and, for each, author an editing instruction that extracts the object and re-places it into a different scene. This explicit scene change mitigates the copy-paste shortcut caused by identical reference and target backgrounds. A high-quality keyframe and each instruction are then passed to an image editor to obtain one reference image per object. Finally, the MLLM produces an R2V caption from the (reference, keyframe) pair.

Person R2V. Image editors often fail to preserve facial identity, so we avoid the editor for human references and instead exploit identity recurrences in long-form video. Clips are first grouped by their parent video or episode, and a face embedding is computed for every clip. For each high-quality target clip, we then retrieve a same-identity reference clip from the same video or episode, with cross-episode filtering to enforce visual diversity. The matched clip is finally downloaded and the person is cropped as a full-body reference image. Sourcing references from real footage rather than editor outputs guarantees identity preservation.

Reference+videos-to-video. RV2V requires triplets (input video, reference, target video) in which the input lacks the referenced object. Since such triplets rarely occur naturally, we synthesize them with a previously trained intermediate-version video editor. For each R2V sample, an MLLM authors an instruction that removes or replaces the referenced object in the target video, and the editor applies it to produce the RV2V input video. The original target and reference complete the triplet.

3.5 Reference-video-guided Video Generation Data

Beyond reference-image-guided video generation and editing, we further explore reference-video-guided settings. Compared with images, videos provide richer temporal information, and therefore we focus in particular on motion transfer. Motion transfer refers to animating the person in an image using the motion of a person in a reference video. Training data for this task requires triplets of (reference video, image, target video). We first extract DWPose [85] from real videos, and then use Bernini’s pose-to-video capability to generate a reference video with the same motion. The reference image is obtained by randomly sampling a frame from the target video. In this way, the triplets required for training can be constructed. Examples of motion transfer data are shown in Fig. 10.



Figure 10 Examples of generated motion-transfer editing data.

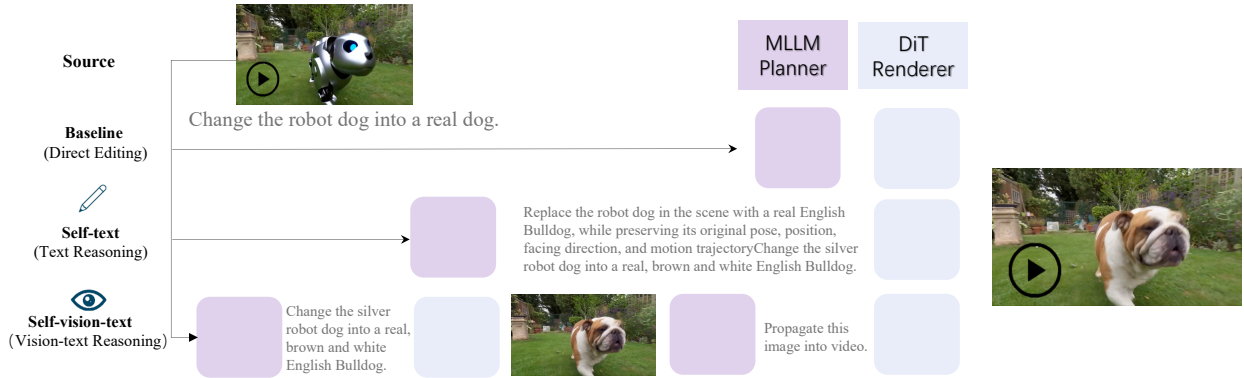


Figure 11 Illustration of our reasoning pattern for reasoning-augmented video editing.

3.6 Reasoning-augmented Video Data

Inspired by recent unified generation methods [15, 73, 80], we incorporate explicit Chain-of-Thought (CoT) reasoning into video editing with an MLLM planner. We consider both self-text reasoning, which rewrites editing instructions into structured intermediate prompts, and self-vision-text reasoning, which introduces visual intermediate states by decomposing video editing into image-level reasoning and video-level generation. This design improves editing fidelity and temporal coherence.

Self-text Reasoning. Large-scale text-only CoT data is constructed to provide explicit reasoning supervision for video editing. The resulting dataset contains approximately 1M samples covering diverse editing tasks, including completion, addition, modification, and reasoning-driven transformations. To build this dataset, an MLLM is prompted with the source video, target video, and original editing instruction. The MLLM is then asked to rewrite the original prompt into a more detailed, structured, and semantically enriched editing instruction, which serves as the explicit reasoning signal.

Self-vision-text Reasoning. While self-text reasoning provides explicit reasoning in the language space, it lacks direct grounding in visual transformations. To overcome this limitation, self vision-text reasoning incorporates visual intermediate states into the reasoning process, decomposing video editing into two stages: image-level reasoning and video-level generation. Given a source video and an editing instruction, the model first performs image editing on the initial frame, guided by textual reasoning, to produce an edited frame that reflects the intended transformation. This edited frame serves as a visual intermediate representation, grounding the reasoning process in the visual domain. Conditioned on this intermediate representation, the model then generates the target video by propagating the edits while preserving temporal consistency. This two-stage formulation bridges spatial reasoning and temporal generation, resulting in improved editing fidelity and

Table 1 Statistics of key generation and editing training data used in the second phase of Stage II and the first phase of Stage III.

Dataset	Weight	Information
<i>T2I — Text-to-Image Generation</i>		
Inhouse T2I	20.00	Internal high-quality text-to-image dataset.
<i>T2V — Text-to-Video Generation</i>		
Inhouse T2V	30.00	Internal high-quality text-to-video dataset.
<i>I2I — Image-to-Image Editing</i>		
UniREdit-100K [25]	1.50	Open-source unified editing dataset.
General-R2I	2.80	Constructed from the general r2v pipeline (Sec. 3.4); key frames as target.
Pico-Banana-400K [57]	4.60	Open-source Pico-Banana 400K single-SFT subset.
Diverse I2I	5.00	Diverse I2I data constructed following the I2I pipeline (Sec. 3.2).
Inhouse I2I	26.10	Internal instruction-based image editing dataset.
<i>I2V — Image / Subject-to-Video Generation</i>		
OpenS2V-Top200K [91]	0.05	Open-source subject-to-video data. We selected 200K high-quality pairs from this, and applied affine transformations to the subject images as data augmentation.
Frame-to-Video	0.15	I2V data conditioned on first, first-last, or first-mid-last frames.
Diverse I2V	0.40	Diverse I2V editing data constructed following the I2V pipeline (Sec. 3.2).
Person-R2V	1.30	Built via the person r2v pipeline (Sec. 3.4).
General-R2V	1.60	Constructed via the general r2v pipeline (Sec. 3.4).
<i>V2V — Video-to-Video Editing</i>		
Video-Extension	0.10	Split video into two parts, take the second part as target video.
Video-Completion	0.10	Split video into three parts, take the middle part as target video.
Senorita-Controllable [99]	0.10	Open-source controllable video editing data.
Sketch-to-Video	0.10	Sketch-conditioned video generation pairs. Sketch is detected with OpenCV Canny.
Inpainting-NoMask	0.10	Mask-free video inpainting pairs. We use GroundingDINO [46] and SAM2 [59] to perform object segmentation.
Colorization	0.10	Video colorization pairs.
Movie-with-Subtitles	0.10	Subtitle-removal pairs from movie clips.
Video2Mask	0.10	Video-to-mask paired data. We use GroundingDINO [46] and SAM2 [59] to perform object segmentation.
Pose2Video	0.15	Pose-conditioned video generation pairs. Human skeleton detection is performed using DWPose [85].
SyncamVideo [1]	0.15	Open-source SynCamVideo-Dataset video data.
TrajectoryCrafter [89]	0.15	Constructed via the Open-source TrajectoryCrafter model.
CameraClone [48]	0.15	Open-source CamCloneMaster video data.
VACE-HQ [31]	0.30	VACE-generated data with human filtering (Sec. 3.3).
Motion-aware Editing	0.60	Constructed via the motion-aware data pipeline (Sec. 3.3).
Propagation-based Editing	1.00	Constructed via the propagation-based data pipeline (Sec. 3.3).
<i>IV2V — Reference-guided Video Editing</i>		
Motion-Transfer	0.10	Constructed via the motion-transfer data pipeline (Sec. 3.5).
Propagation	0.40	Propagation data built from V2V first-frame extraction.
Motion-aware Editing Ref	0.60	Constructed from motion-aware editing data by using an image editing model to extract the edited object from the first frame as the reference image.
Propagation-based Editing Ref	1.05	Constructed from Propagation-based Editing data by using an image editing model to extract the edited object from the first frame as the reference image.
Person-RV2V	1.05	Person-centric RV2V replacement data.

temporal coherence.

As illustrated in Fig. 11, our self-text reasoning refines and expands upon the initial editing instruction. Furthermore, our self-vision-text reasoning introduces an intermediate visual state to guide the video editing process, providing explicit visual grounding. Both approaches offer richer contextual information than the baseline method.

4 Training and Inference

Table 2 Training settings across different stages, where Res. denotes resolution, V.P. denotes video pairs, I.P. denotes image pairs, Int. denotes interleaved image-text data, Und. denotes understanding data, and CoT denotes reasoning-augmented video data.

Stage	Optimized	Res.	LR	EMA	T2I	T2V	I2I	V2V	I2V	IV2V	V.P.	I.P.	Int.	Und.	CoT
I	MLLM	256p	1e-5	0.999	13%	19%	3%	1%	1%	1%	15%	21%	6%	20%	-
II	DiT	480p	1e-5	0.9995	31%	42%	4%	0.4%	0.4%	0.3%	11%	11%	-	-	-
	DiT	480p	1e-5	0.9999	20%	30%	40%	3.3%	3.5%	3.2%	-	-	-	-	-
III	All	480p	1e-5	0.9995	16%	24%	32%	2.6%	2.8%	2.6%	-	-	-	20%	-
	All	480p	1e-5	0.999	12%	18%	24%	2%	2%	2%	-	-	-	20%	20%

4.1 Training Pipelines

To fully exploit the understanding capability of the MLLM and the synthesis capability of the diffusion model, we adopt a three-stage training pipeline as shown in Table 2. The composition of the key generation and editing data is summarized in Table 1. We first train the MLLM-based planner and the DiT-based renderer separately, and then lightly co-train them to align semantic planning with visual rendering. This design preserves the strengths of both components while avoiding excessive interference during early training.

Stage I: MLLM pretraining. In Stage I, we train the MLLM planner together with the ViT embedding decoder to predict target visual semantics in the ViT embedding space. Training is conducted with the joint objective $\lambda_{\text{text}}\mathcal{L}_{\text{ntp}} + \lambda_{\text{visual}}\mathcal{L}_{\text{visual}}$, where $\lambda_{\text{text}} = 0.2$ and $\lambda_{\text{visual}} = 1$. The goal of this stage is to transform the MLLM from a pure understanding model into a semantic planner that can infer target visual representations from multimodal context.

Training follows a progressive data curriculum. Large-scale text-to-image data is used first to establish image generation ability in the semantic space. The training corpus is then expanded to include text-to-video, image-pair, and video-pair data, enabling the planner to model not only image and video generation, but also image and video editing within a unified semantic space. To preserve the pretrained language and multimodal reasoning capabilities of the MLLM, multimodal understanding data and text understanding data are further incorporated at this stage. Training is performed at 256P resolution and 2 fps.

To improve robustness across heterogeneous tasks, we adopt a task-dependent mask ratio strategy. Specifically, the mask ratio $r \in [0, 1]$ is randomly sampled from a Beta distribution,

$$r \sim \text{Beta}(\alpha, \beta), \quad (5)$$

where (α, β) are specified for each task. This design provides a flexible way to control the amount of visible target information under different training objectives. As the task input becomes more informative, e.g., from text-only generation to image/video-conditioned editing, we gradually increase α and decrease β , which shifts the distribution of r toward probability 1.0. As a result, a larger portion of target visual tokens is masked during training, reducing information leakage from the visible target tokens and forcing the planner to infer the masked semantics from higher-level multimodal context. This strategy is particularly important for editing tasks, where the source input is highly correlated with the target and may otherwise make semantic prediction overly easy. The detailed configuration is summarized in Table 3.

Overall, Stage I equips the planner with broad semantic prediction ability across heterogeneous generation, editing, and understanding tasks, while the task-dependent mask ratio further improves its robustness under diverse semantic completion difficulties.

Stage II: DiT pretraining. In Stage II, we train the DiT-based renderer, together with its lightweight text encoder, e.g., T5, to endow it with strong generation and editing ability before coupling it with the MLLM planner. The renderer is optimized with \mathcal{L}_{dit} and conditioned on text features and source VAE features, allowing it to learn both high-fidelity synthesis and source-preserving editing.

In this stage, the renderer is trained on a large mixture of text-to-image, text-to-video, editing, image-pair, and video-pair data. While pair data is particularly beneficial for improving generalization and editing quality,

Table 3 Mask ratio configuration during MLLM planner training. The mask ratio is sampled from a task-dependent Beta distribution $\text{Beta}(\alpha, \beta)$.

Parameter	T2I	T2V	I2I	I2V	V2V	IV2V
α	5.0	8.0	8.0	10.0	12.0	12.0
β	1.1	1.05	1.05	1.0	0.9	0.9

Table 4 Training noise scheduler configuration.

Parameter	T2I	I2I	T2V	I2V	V2V	IV2V
Weighting	logit-normal	logit-normal	mode	mode	mode	mode
Shift	3.0	4.0	3.0	5.0	5.0	5.0

it may also lead to weaker instruction following and inconsistencies in non-edited regions. We therefore adopt a linearly decayed sampling strategy for pair data, using a high ratio at the beginning of training and gradually reducing it to zero, such that the later stage relies on high-quality editing data to refine editing performance. Training in this stage is performed at 480P and 16 fps.

To accommodate the varying optimization dynamics across these distinct tasks, we assign customized shift parameters and noise weighting schemes for each individual task, as summarized in Table 4. Following SD3 [20] and Waver [94], the logit-normal and mode functions, are used for timestep sampling, as is shown in Eq. 6 and Eq. 7, respectively. We adopt $\text{Lognorm}(0.5, 1)$ for the image related tasks, $\text{Mode}(1.29)$ for the video related tasks.

$$\pi_{\text{In}}(t; m, s) = \frac{1}{s\sqrt{2\pi}} \frac{1}{t(1-t)} \exp\left(-\frac{(\text{logit}(t) - m)^2}{2s^2}\right), \quad (6)$$

$$f_{\text{mode}}(u; s) = 1 - u - s \cdot \left(\cos^2\left(\frac{\pi}{2}u\right) - 1 + u\right). \quad (7)$$

Stage III: Joint training. In Stage III, we jointly train the MLLM planner and the DiT renderer to align semantic planning and visual rendering within a unified framework. The model is optimized using the objective in Eq 3, with $\lambda_{\text{ntp}} = 0.2$ and $\lambda_{\text{visual}} = \lambda_{\text{dit}} = 1$. This stage connects the planner’s semantic predictions in the ViT embedding space with the renderer’s synthesis process in the VAE latent space, enabling the full system to perform planning before rendering. Specifically, during training, the text, source ViT tokens, and masked target ViT tokens are fed into the MLLM. The MLLM hidden states corresponding to the text, source ViT tokens, and unmasked target ViT tokens are extracted as the conditioning input for the diffusion model. Meanwhile, the hidden states corresponding to the masked target ViT tokens are fed into the ViT embedding decoder, where $\mathcal{L}_{\text{visual}}$ is computed.

Joint training is conducted at 480P and 16 fps on a mixture of high-quality image and video generation/editing data together with text-only and multimodal understanding data. The understanding data helps preserve the MLLM’s language and multimodal reasoning capabilities, while the generation and editing data encourage the emergence of a stable semantic-to-visual interface between the planner and the renderer. In the later phase of joint training, we additionally introduce reasoning-augmented Chain-of-Thought (CoT) data to enhance structured reasoning for video editing. This encourages the model to perform more explicit semantic planning over object dynamics, temporal transitions, and editing intent before rendering the final output.

Compared with the separate pretraining stages, Stage III uses only light co-training for a relatively small number of steps. This is sufficient to align the planner and renderer while preserving the pretrained strengths of both. As a result, the MLLM retains strong understanding and reasoning ability, the renderer preserves high-fidelity generation and editing performance, and the overall system learns to translate multimodal reasoning into faithful visual outputs.

Table 5 Inference guidance scales for different tasks.

Task	Steps	ω_{txt}	ω_{vid}	ω_{img}	ω_{tgt}
T2V	60	4.0	–	1.0	1.0
S2V	40	4.0	1.25	2.5	1.5
V2V	40	4.0	1.25	1.25	0.5
RV2V	40	4.0	1.25	3.0	1.5

4.2 Inference Strategy

ViT embedding planning via MLLM. During inference, the target visual tokens are initialized as masked, and the MLLM progressively predicts the target semantic tokens following standard masked generative inference [8, 39]. Unless otherwise specified, we use 25 iterative planning steps to predict the full target semantic embedding sequence. At each planning step, the predicted semantic features are decoded into target ViT embeddings by the ViT embedding decoder via flow matching, where the decoder performs 5 diffusion denoising steps in the ViT embedding space. For this diffusion refinement stage, the text and image guidance scales are set to 1.2 and 1.0, respectively.

After all target ViT embeddings are obtained, they are fed back into the MLLM together with the textual embedding and source ViT embeddings to produce contextualized hidden states for conditioning the DiT-based renderer. In practice, the iterative inference of the MLLM-based planner introduces only negligible overhead compared with the subsequent DiT rendering stage, with runtime that is almost negligible relative to the DiT renderer. This indicates that the additional cost of multi-step semantic planning is negligible relative to the overall diffusion sampling cost, while still providing high-quality semantic guidance for downstream rendering.

Visual target rendering via DiT. The DiT-based renderer performs latent-space denoising under multi-source guidance from source video VAE features, source image VAE features, text features, and target semantic embeddings. The flow shift is set to 5.0 for the DiT-based renderer. The renderer performs 60 denoising steps for text-to-video generation and 40 denoising steps for subject-to-video generation, video-to-video editing, and reference-guided video-to-video editing.

To control the contribution of different conditions, we decompose the final prediction into an unconditional base term and four incremental guidance terms associated with the source video VAE features, source image VAE features, text features, and target semantic embeddings, respectively. Specifically, let $\epsilon_{\emptyset, \emptyset, \emptyset, \emptyset}$ denote the prediction without any condition, $\epsilon_{\emptyset, \emptyset, \text{vid}, \emptyset}$ the prediction conditioned only on the source video VAE features, $\epsilon_{\emptyset, \emptyset, \text{vid}, \text{img}}$ the prediction conditioned on both source video and source image VAE features, $\epsilon_{\text{txt}, \emptyset, \text{vid}, \text{img}}$ the prediction additionally conditioned on text features, and $\epsilon_{\text{txt}, \text{tgt}, \text{vid}, \text{img}}$ the prediction further conditioned on target semantic embeddings. The incremental contributions are defined as

$$\Delta_{\text{vid}} = \epsilon_{\emptyset, \emptyset, \text{vid}, \emptyset} - \epsilon_{\emptyset, \emptyset, \emptyset, \emptyset}, \quad (8)$$

$$\Delta_{\text{img}} = \epsilon_{\emptyset, \emptyset, \text{vid}, \text{img}} - \epsilon_{\emptyset, \emptyset, \text{vid}, \emptyset}, \quad (9)$$

$$\Delta_{\text{txt}} = \epsilon_{\text{txt}, \emptyset, \text{vid}, \text{img}} - \epsilon_{\emptyset, \emptyset, \text{vid}, \text{img}}, \quad (10)$$

$$\Delta_{\text{tgt}} = \epsilon_{\text{txt}, \text{tgt}, \text{vid}, \text{img}} - \epsilon_{\text{txt}, \emptyset, \text{vid}, \text{img}}. \quad (11)$$

Accordingly, the final prediction is

$$\hat{\epsilon} = \epsilon_{\emptyset, \emptyset, \emptyset, \emptyset} + \omega_{\text{vid}} \Delta_{\text{vid}} + \omega_{\text{img}} \Delta_{\text{img}} + \omega_{\text{txt}} \Delta_{\text{txt}} + \omega_{\text{tgt}} \Delta_{\text{tgt}}, \quad (12)$$

where ω_{vid} , ω_{img} , ω_{txt} , and ω_{tgt} are the corresponding guidance scales for source video VAE features, source image VAE features, text features, and target semantic embeddings, respectively. We further apply adaptive projected guidance [62] to reduce oversaturation.

The guidance scales used by the DiT-based renderer for different tasks are summarized in Table 5. For text-to-video generation, where no source video is provided, the source video guidance term is not used.

5 Infrastructure

5.1 Training Infrastructure

Training long-context video editing models with co-trained DiT and MLLM components posed substantial systems challenges in memory, computation, parallelism, and data loading. On the memory side, we optimized FSDP configurations and restructured the input pipeline to use direct index-scattering into pre-allocated buffers, reducing per-GPU memory from 72 GB to 40 GB. Combined with a custom activation offloading pipeline with pinned CPU memory pools and delayed-queue prefetch, these took a $4.4\times$ improvement for training sequence length. On the computation side, kernel-level optimizations including FlashAttention-4 [92], asynchronous QKV communication, TND memory layout preservation, and a high-performance RMSNorm kernel [14] collectively yielded up to 46% speedup. For parallelism, we adopted Ulysses-style sequence parallelism [30] for both DiT and MLLM, extending it to selectively unfrozen MLLM in joint training. We further implemented sequence packing with token-bucket batching and greedy bin-packing data loading to handle heterogeneous sequence lengths, together improving end-to-end throughput by $\sim 4.5\times$.

Memory Optimization. Video editing training involved extremely long sequences that imposed severe GPU memory pressure. We systematically profiled and optimized FSDP configurations, reducing per-GPU memory from 72 GB to 40 GB. Beyond FSDP tuning, we restructured the input preparation pipeline: instead of first concatenating all visual and textual tokens and then scattering them to target positions for sequence parallel, we directly index-scattered tokens into pre-allocated buffers, eliminating 17 GB of intermediate memory allocation. For stage III, we implemented a custom activation offloading pipeline with a pinned CPU memory pool and a delayed-queue prefetch mechanism, overlapping D2H/H2D transfers with computation. Combined with padding and normalization optimizations, these strategies enabled stable training with 440K-token sequences—a $4.4\times$ improvement over the previous 100K-token limit.

High-Performance Operators and Pipelines. We performed systematic, kernel-level optimizations tailored for our target GPU architecture. Key optimizations included applying FlashAttention-4 [92] in the DiT and FlexAttention [17] in the MLLM, implementing an asynchronous QKV communication pipeline, and eliminating redundant cross-attention communication. Furthermore, we maintained the TND memory layout to avoid costly transposes and placed `cu_seq1ens` tensors on the CPU to reduce device memory pressure. We also adopted the high-performance RMSNorm kernel from QuACK [14], which yielded an additional 5–10% end-to-end training speedup. A unified attention backend ensures seamless deployment across heterogeneous GPU clusters.

Parallelism Strategy. We employed FSDP for memory-efficient weight sharding combined with Ulysses-style sequence parallelism [30] for both DiT and MLLM components. For the DiT-based Renderer, sequence parallelism sharded tokens across GPUs along the sequence and head dimensions, enabling the processing of long video sequences. For the MLLM-based Planner, we extended Ulysses SP, achieving $2\times$ throughput at SP degree 4. SP was enabled only for long-sequence tasks to avoid unnecessary communication overhead on shorter inputs.

Sequence Packing and Batch Forward. To improve GPU utilization under heterogeneous sequence lengths, we implemented a comprehensive sequence packing pipeline. Training samples were first sorted by sequence length for each sequence parallel group, achieving a $2\times$ throughput speedup. We then introduced batch forward for both MLLM and diffusion components: MLLM inputs were batched with FlashAttention variable-length kernels, while diffusion inputs were concatenated and processed jointly. To avoid cross-rank deadlocks caused by varying local batch sizes, we applied dummy-forward padding to ensure consistent execution across all ranks. We further introduced token-bucket batching, which grouped samples into discrete length buckets and applied per-bucket loss re-weighting to eliminate padding waste while preserving training dynamics. Together, these optimizations improved end-to-end throughput by $\sim 4.5\times$.

Dataloader Balance. Large-scale video editing training involved highly heterogeneous data, including varying video lengths, resolutions, and editing operations, which introduced significant computational imbalance across GPUs. We implemented a load-balanced data loader using greedy bin-packing to redistribute workloads across nodes at each iteration, achieving a max/min workload ratio below 1.01 and approximately 15% throughput improvement.

5.2 Inference Parallelism

We adopted multi-GPU inference to further reduce latency. For the DiT model, we integrated DeepSpeed Ulysses [30] with asynchronous all-to-all communication for the QKV tensor. For the VAE module, we employed context parallelism along the temporal dimension with asynchronous conv cache transmission. Together, these achieved a speedup of over $7.2\times$.

5.3 Model Distillation

To reduce the sampling cost of our diffusion model while preserving generation quality, we adopted a two-stage distillation strategy. In the first stage, we performed CFG distillation [51], which trained a student model to directly predict the CFG-combined output in a single forward pass, eliminating the need for dual (conditional and unconditional) evaluations at each sampling step and halving the per-step compute. In the second stage, we applied ReFlow [47], which straightened the learned probability flow ODE trajectories, enabling accurate generation with significantly fewer integration steps. By progressively reducing both per-step cost and the total number of required steps, this two-stage pipeline achieved substantial end-to-end inference speedup with minimal quality degradation. Finally, the distilled student model with only 4 NFEs achieved comparable quality to the teacher model with 80 NFEs.

6 Experiments

We evaluate Bernini on two complementary task families that together cover its capabilities as a unified framework: video editing and video generation. To enable a more comprehensive evaluation of video editing capabilities, we introduce Bernini-Bench (Sec. 6.2). Then we present main results on video editing (Sec. 6.3) and analyze the contribution of reasoning-augmented editing (Sec. 6.4), followed by results on video generation (Sec. 6.5). We also conduct ablation studies (Sect. 6.6) and discuss the generalizability of Bernini (Sect. 6.7).

6.1 Implementation Details

Qwen2.5-VL-7B [69] is adopted as the MLLM-based planner, and Wan2.2-A14B [70] serves as the DiT-based renderer. To better align with the pretrained conditioning distribution of Wan2.2, we retain the original T5 features in the textual condition of the DiT renderer. Specifically, only the penultimate-layer hidden states of the MLLM are passed through a lightweight zero-initialized one-layer MLP, and the projected features are then concatenated with the T5 features to form the final conditioning input. This design preserves Wan2.2’s pretrained text-conditioning prior while introducing higher-level semantic guidance from the MLLM. Unless otherwise specified, following prior work [68], we enhance the user instruction with an additional multimodal large language model and feed the rewritten instruction into Bernini to further improve performance.

6.2 Bernini-Bench

Benchmark Construction. Currently, prevalent video editing benchmarks, such as OpenVE-Bench [26] and EditVerse [32], predominantly focus on video-to-video editing, neglecting the video+image-to-video paradigm. Moreover, these benchmarks are relatively limited in both the diversity of editing types and the variety of video content. To provide a more comprehensive evaluation of video editing models, we manually build Bernini-Bench, a new benchmark for assessing editing performance across diverse task types and real-world scenarios. Bernini-Bench covers two input settings, *text-guided video-to-video editing (V2V)* and *reference-image-guided video editing (RV2V)*. It comprises 300 test cases spanning 22 editing categories, including action editing, position editing, edits involving causal reasoning, and edits with changes in camera focus, which are editing types not covered by other benchmarks. For each editing category, 10 cases were carefully selected, each accompanied by rich editing instructions (e.g., a wide range of target styles for style transfer). To better reflect real-world applications, we collected source videos from several free and open-source stock media platforms. The selected videos cover diverse editing-relevant attributes, including variations in human composition, shot scale, scene environment, camera motion, and visual complexity, and include both horizontal and vertical aspect ratios. The detailed statistics of Bernini-Bench are presented in Fig. 12.

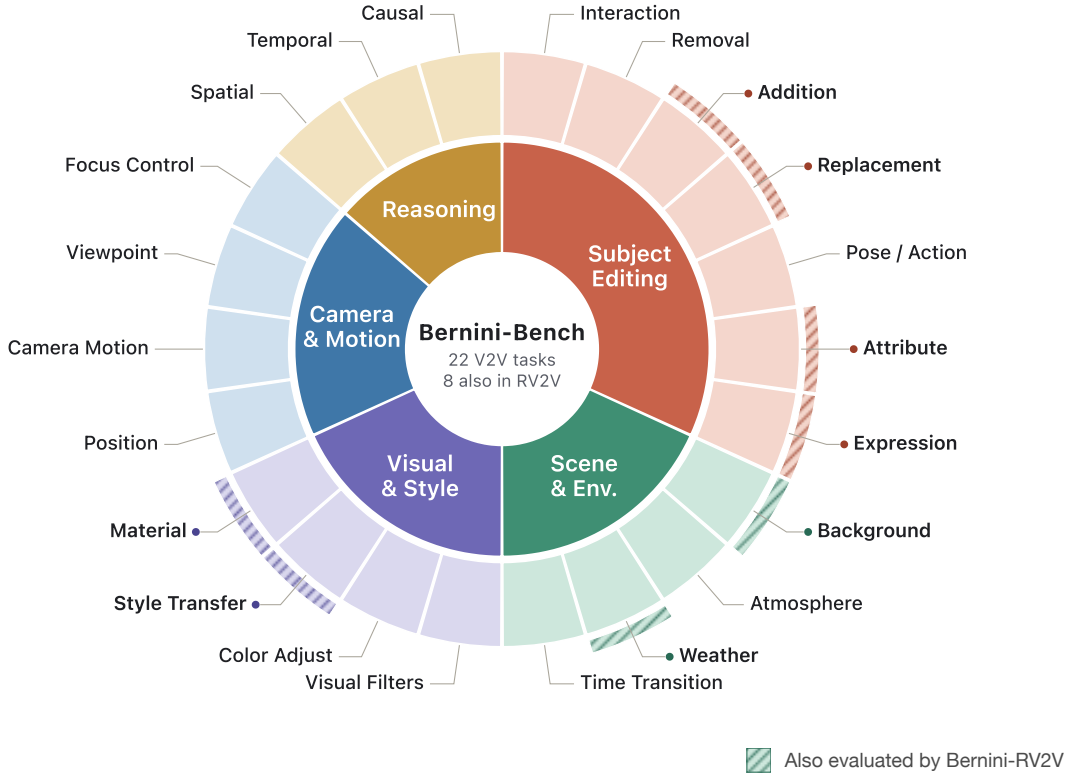


Figure 12 Overview of Bernini-Bench. Our benchmark spans 22 fine-grained V2V editing tasks across five dimensions: Subject Editing, Scene & Environment, Visual & Style, Camera & Motion, and Reasoning. Hatched segments denote the 8 tasks also evaluated under the reference-video-to-video (Bernini-RV2V) setting.

Evaluation Metrics. Similarly to existing video editing benchmarks [26, 32], we evaluate the model performance across five dimensions: instruction following, source video consistency, reference image consistency, generation quality and overall score. For a comprehensive performance evaluation, all dimensions (excluding overall performance) are set to be as orthogonal as possible for independent assessment. The specific criteria are as follows:

- **Instruction Following (IF):** Evaluates the model’s ability to accurately and faithfully execute textual editing instructions, such as correctly identifying the editing target and operation type.
- **Video Consistency (VC):** Measures whether the non-edited regions of the video remain consistent before and after editing.
- **Reference Image Consistency (IC):** Assesses the consistency of visual features (shape, color, texture, style) between the editing result and the given reference image. This metric is evaluated only for the RV2V task.
- **Generation Quality (GQ):** Focuses on the video’s physical realism, edited content naturalness, as well as the presence of severe AI artifacts and obvious visual distortion.
- **Overall Score (OS):** Evaluates whether the editing result meets the user’s expectations.

For actual evaluation, we adopt two approaches for each dimension: MLLM-based scoring, and human Side-by-Side (SBS) comparison. For MLLM-based scoring, the model assigns a score ranging from 1 to 5 for each evaluation dimension. Specifically, samples where the model fails to respond to the instruction at all are excluded from the final score calculation for source video consistency, reference image consistency, and generation quality. Since current MLLMs are unable to accurately judge issues such as small-scale distortions or unnatural artifacts when assessing generation quality, the corresponding results should be treated as for

Table 6 Quantitative results on Bernini-V2V and RV2V.

Method	Bernini-V2V				Bernini-RV2V				
	OS	IF	VC	GQ	OS	IF	VC	IC	GQ
UniVideo [76]	2.44	2.58	3.30	3.16	2.36	2.67	3.15	2.87	2.82
VINO [9]	2.85	3.08	3.14	3.26	2.25	2.64	2.17	3.51	3.06
Kling O3 [68]	3.05	3.25	3.09	3.44	3.14	3.41	3.14	<u>3.61</u>	3.30
Wan2.7 [70]	<u>3.30</u>	<u>3.57</u>	<u>3.11</u>	3.56	3.58	3.82	<u>3.48</u>	3.62	3.43
Bernini	3.49	3.66	3.51	<u>3.49</u>	<u>3.50</u>	<u>3.75</u>	3.51	3.54	<u>3.31</u>

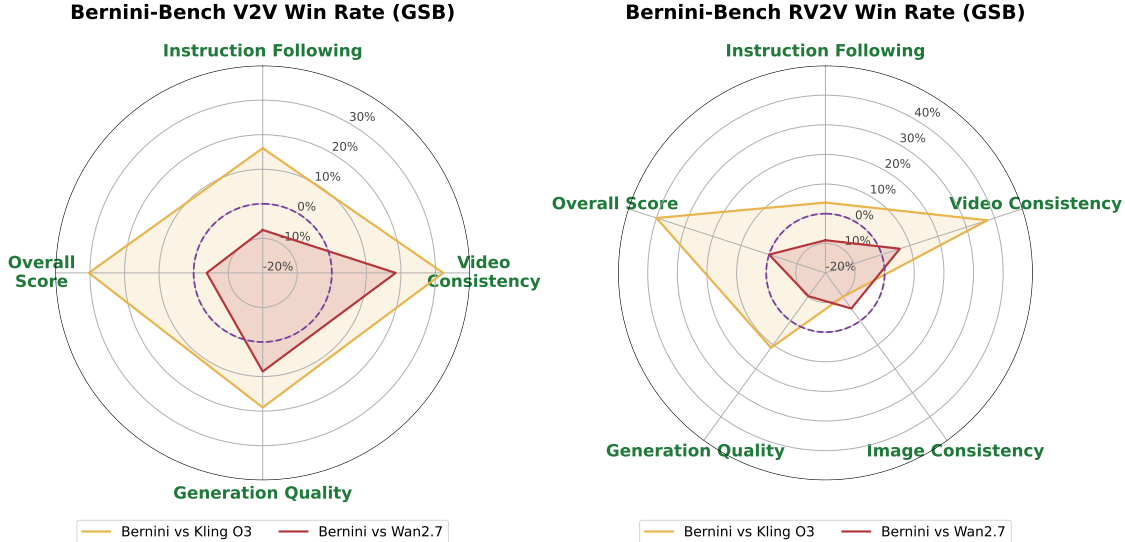


Figure 13 GSB win rates on Bernini-Bench. Relative win rates $((\text{God} - \text{Bad}) / \text{Total})$ of Bernini against Kling O3 and Wan2.7 on V2V (left) and RV2V (right).

reference only. We use GPT-5.4-2026-03-05 for evaluation. The detailed prompts used for MLLM scoring can be found in the Appendix A.

6.3 Video Editing

MLLM Evaluation on Bernini-Bench. For fair comparison, the outputs of Kling O3 and Wan2.7 are downsampled to 480p at 16 fps, matching Bernini’s generation setting. As shown in Table 6, Bernini achieves the best overall performance on Bernini-V2V, raising the overall score from 3.30 to 3.49 compared with Wan2.7. Relative to Kling O3, it consistently outperforms across all evaluation dimensions. Relative to Wan2.7, Bernini is comparable in instruction following and generation quality, but shows a markedly stronger ability to preserve video consistency. On Bernini-RV2V, Bernini again achieves the best video consistency and remains competitive on the other metrics. These results show that Bernini is able to preserve consistency in non-edited regions to the greatest extent possible while correctly executing the instruction, which is often overlooked by existing editing models.

Human Side-By-Side Evaluation on Bernini-Bench. As shown in Fig. 13, we present the results of side-by-side (SBS) human evaluation conducted on the Bernini-Bench. Compared with the scores from MLLM-based automatic evaluation, human evaluation can more accurately reflect the actual performance of different models. Bernini outperforms Kling O3 across most evaluation dimensions, and achieves competitive performance on par with Wan2.7. In particular, Bernini exhibits a significant advantage in terms of Video Consistency.

Evaluation on Public Benchmarks. We evaluate Bernini on three public video editing benchmarks: OpenVE [26],

Table 7 Quantitative Comparison on OpenVE-Bench with Gemini 2.5 pro.

Method	Overall \uparrow	Global Style	Background Change	Local Change	Local Remove	Local Add	Subtitle Edit	Creative Edit	Camera Edit
VACE-14B [31]	1.57	1.49	1.55	2.07	1.46	1.26	1.48	1.47	1.62
OmniVideo [66]	1.31	1.11	1.18	1.14	1.14	1.36	1.00	2.26	1.00
InsViE [81]	1.53	2.20	1.06	1.48	1.36	1.17	2.18	2.02	1.09
Ditto [3]	1.98	4.01	1.68	2.03	1.53	1.41	2.81	1.23	1.32
ICVE [41]	2.07	2.22	1.62	2.57	2.51	1.97	2.09	2.41	1.11
Lucy-Edit [67]	2.15	2.27	1.57	3.20	1.75	2.30	1.61	2.86	1.61
OpenVE-Edit [26]	2.49	3.16	2.36	2.98	1.85	2.15	<u>2.91</u>	2.31	2.02
VINO [9]	<u>3.18</u>	<u>4.34</u>	<u>2.54</u>	<u>3.73</u>	<u>3.22</u>	<u>2.77</u>	2.61	<u>3.29</u>	<u>2.81</u>
Bernini	4.04	4.45	3.31	4.85	4.16	3.43	3.57	3.91	4.67

Table 8 Comparison of video editing methods on EditVerse.

Method	VLM evaluation	Video Quality	Text Alignment		Temporal Consist.	
	Editing Quality \uparrow	Pick Score \uparrow	Frame \uparrow	Video \uparrow	CLIP \uparrow	DINO \uparrow
TokenFlow [23]	5.26	19.73	25.57	22.70	98.36	98.09
STDF [87]	4.41	19.45	25.24	22.26	96.04	95.22
Señorita-2M [99]	6.97	19.71	26.34	23.24	98.05	97.99
InsV2V [12]	5.21	19.39	24.99	22.54	97.15	96.57
Lucy-Edit [67]	5.89	19.67	26.00	23.11	98.49	<u>98.38</u>
EditVerse [32]	<u>7.65</u>	<u>20.07</u>	<u>26.73</u>	<u>23.93</u>	98.56	98.42
Bernini	8.02	20.26	27.37	24.62	<u>98.55</u>	98.37

Table 9 Quantitative Comparison on FiVE Benchmark [37].

Method	Structure	Background Preservation			Text Alignment		Motion	FiVE				
	Dist. $\times 10^3 \downarrow$	PSNR \uparrow	LPIPS $\times 10^3 \downarrow$	SSIM $\times 10^2 \uparrow$	CLIPS. \uparrow	CLIPS. _{edit} \uparrow	Fid S. $\times 10^2 \uparrow$	YN \uparrow	MC \uparrow	U \uparrow	$\cap \uparrow$	Acc \uparrow
Source Videos	0.00	∞	0.00	100.00	24.59	19.87	93.76	–	–	–	–	–
TokenFlow	35.62	19.06	263.61	72.51	26.46	21.15	89.00	19.36	35.51	36.68	18.18	27.43
DMT	85.95	14.71	404.60	51.64	26.66	<u>21.44</u>	82.30	34.78	62.06	62.98	33.86	48.42
VidToMe	22.37	21.15	263.91	70.69	26.84	21.05	90.06	20.03	33.50	36.20	17.34	26.77
AnyV2V	71.36	15.90	348.59	50.77	24.89	19.72	60.36	30.62	45.42	48.96	27.09	38.02
VideoGrain	12.40	27.05	<u>185.21</u>	79.13	25.69	20.31	88.57	30.50	43.97	44.30	30.17	37.23
Pyramid-Edit	28.65	20.84	276.59	71.72	26.82	20.20	80.59	33.67	54.01	56.36	31.31	43.84
Wan-Edit	<u>12.53</u>	25.57	94.61	<u>82.55</u>	26.39	21.23	<u>89.43</u>	41.41	52.53	55.72	38.22	46.97
Omni	34.94	22.95	217.55	73.78	<u>26.92</u>	21.19	84.22	<u>62.83</u>	<u>81.81</u>	<u>84.33</u>	<u>60.23</u>	<u>72.41</u>
Bernini	13.54	<u>26.35</u>	207.89	84.38	27.75	22.74	86.27	71.33	84.98	87.67	68.65	78.16

EditVerse [32], and FiVE [37]. As shown in Tables 7, 8, and 9, Bernini consistently delivers strong performance across diverse evaluation settings. On OpenVE, it outperforms the strongest baseline VINO by a large margin in overall score (4.04 vs. 3.18). On EditVerse, Bernini achieves the best editing quality, pick score, and text alignment, especially setting a new high score of 8.02 on editing quality. On FiVE, Bernini attains state-of-the-art or near-state-of-the-art performance across structure, background, alignment, and editing accuracy metrics, with particularly strong results on the VQA-based FiVE-Acc metrics, indicating more faithful realization of the target edits.

Qualitative Comparison. Figure 14 presents a qualitative comparison between Bernini and existing state-of-the-art video editing models. In the V2V case of modifying the puppy’s motion, VINO produces a puppy that is inconsistent with the original video, Kling-O3 generates a background that does not match the original video, and Wan-2.7 produces obvious distortion in the puppy on the left. Only Bernini preserves both the puppy and the background consistently with the original video while naturally modifying the puppy’s motion. In the case of adding a person, Kling-O3 successfully adds a person, but the added character sits stiffly.



Figure 14 Qualitative comparison of Bernini with SoTA methods on V2V and RV2V tasks.

Table 10 Comparison of reasoning variants on the Bernini-V2V benchmark. PE means a Prompt Enhancer that maps diverse user prompts onto a distribution that is consistent with the model’s training data.

Method	OS	IF	VC	GQ
Ours (baseline)	3.12	3.36	3.18	3.37
+ PE (Qwen2.5-VL-7B [69])	3.20	3.43	3.21	3.39
+ Self-text	3.33	3.55	3.31	3.44
+ PE (GPT-5.4)	<u>3.49</u>	3.66	<u>3.51</u>	3.49
+ PE (GPT-5.4) + Self-visual-text	3.52	<u>3.65</u>	3.54	3.49

Both Wan-2.7 and Bernini not only add a new person but also enable natural interaction between the new character and the two original girls; however, Wan-2.7 incorrectly introduces an extra blue seat cushion in the middle. In the first RV2V case, only Bernini successfully preserves the identity consistency of the person in the video while modifying the facial expression. In the second RV2V case, only Bernini generates a boat that is consistent with the one in the reference image. More results are shown in Appendix B.1.

6.4 Reasoning-augmented Video Editing

Table 10 presents the results on the Bernini-V2V benchmark. Overall, enriching the reasoning context consistently improves performance. First, we use Qwen2.5-VL-7B, the initialization model of our MLLM planner, as a Prompt Enhancer to refine the input prompts. Although this brings slight improvements over the baseline, it performs worse than our self-text reasoning approach, indicating that our model develops stronger textual reasoning capabilities beyond its initialization model. To further explore the upper bound of textual reasoning, we employ a stronger Prompt Enhancer GPT-5.4, which achieves consistent gains across most metrics. Building on this, incorporating vision-text reasoning achieves the best overall performance, showing that multimodal reasoning provides complementary benefits beyond text-only reasoning. Detailed qualitative comparisons are provided in Appendix B.2.

Table 11 Quantitative comparison on VBench [29].

Method	Total \uparrow	Quality score	Semantic score	Aesthetic quality	Dynamic degree	Object class	Overall consist.
<i>Closed-source systems</i>							
Sora [53]	84.28	85.51	79.35	63.46	<u>79.91</u>	93.93	26.26
Veo3 [24]	85.06	85.70	<u>82.49</u>	63.81	72.43	93.89	27.88
Kling 1.6 [34]	83.40	85.00	76.99	64.81	62.22	93.34	26.04
Jimeng [6]	81.97	83.29	76.69	68.80	38.43	89.62	27.10
Gen-3 [61]	82.32	84.11	75.17	63.34	60.14	87.81	26.69
<i>Open-source systems</i>							
StepVideo [49]	81.83	84.46	71.28	61.23	53.06	80.56	27.12
CogVideoX-5B [86]	81.91	83.05	77.33	61.88	69.51	85.07	27.65
Wan2.1-14B [70]	83.69	<u>85.59</u>	76.11	66.07	65.46	86.28	25.91
HunyuanVideo [33]	83.24	85.09	75.82	60.36	70.83	86.10	26.44
VINO [9]	83.17	83.69	81.08	<u>68.11</u>	55.56	91.17	27.00
Wan2.2-A14B	<u>84.79</u>	85.33	82.61	67.06	69.72	96.00	27.36
Bernini	84.64	85.18	<u>82.49</u>	64.68	81.11	<u>95.41</u>	<u>27.83</u>

Table 12 OpenS2V open-domain results on subject-to-video generation. Higher is better for all metrics.

Method	Total	Aesth.	Motion Smooth.	Motion Ampl.	FaceSim	GmeScore	NexusScore	NaturalScore
<i>Closed-source systems</i>								
Pika 2.1 [56]	51.88	46.88	87.06	24.71	30.38	69.19	45.40	63.32
Vidu 2.0 [63]	51.95	41.48	90.45	13.52	35.11	67.57	43.37	65.88
Kling 1.6 [34]	56.23	44.59	86.93	41.60	40.10	66.20	45.89	74.59
Kling O3 [34]	59.19	48.05	92.94	24.47	<u>57.20</u>	66.44	45.53	70.51
<i>Open-source systems</i>								
SkyReels-A2 [21]	52.25	39.41	87.93	25.60	45.95	64.54	43.75	60.32
MAGREF [16]	52.51	45.02	93.17	21.81	30.83	<u>70.47</u>	43.04	66.90
Phantom-14B [45]	56.77	46.39	<u>96.31</u>	<u>33.42</u>	51.46	70.65	37.43	69.35
VACE-14B [31]	57.55	<u>47.21</u>	94.97	15.02	55.09	67.27	44.08	67.04
VINO [9]	57.85	45.92	94.73	12.30	52.00	69.69	42.67	71.99
Saber [98]	57.91	42.42	96.12	21.12	49.89	67.50	<u>47.22</u>	72.55
RefAlign-14B [72]	<u>60.42</u>	46.84	97.61	22.48	55.23	68.32	48.52	<u>73.63</u>
Bernini	62.94	44.14	93.66	23.39	78.20	65.35	46.95	70.51

6.5 Video Generation

Text-to-Video Generation. We evaluate Bernini on VBench [29] to assess its text-to-video generation capability. As Bernini is built on top of Wan2.2-A14B and extends it to a unified framework that additionally supports video editing and subject-to-video generation, we compare against Wan2.2-A14B to examine how the text-to-video capability is retained after this extension. As shown in Table 11, Bernini reaches a Total score of 84.64, essentially matching Wan2.2-A14B (84.79). These results indicate that the unified design of Bernini broadens the model’s capability across editing and reference-based generation tasks while retaining the base text-to-video quality.

Subject-to-Video Generation. We evaluate our method on OpenS2V-Eval [91], a benchmark for multi-reference subject-to-video generation spanning humans, objects, and face-identity consistency. Following its evaluation protocol, we report the overall Total score together with all sub-metrics defined therein. As summarized in Table 12, our method achieves the highest Total score of **62.94**, surpassing all closed-source and open-source competitors, including the strongest prior results from Kling O3 (59.19) and RefAlign-14B (60.42).

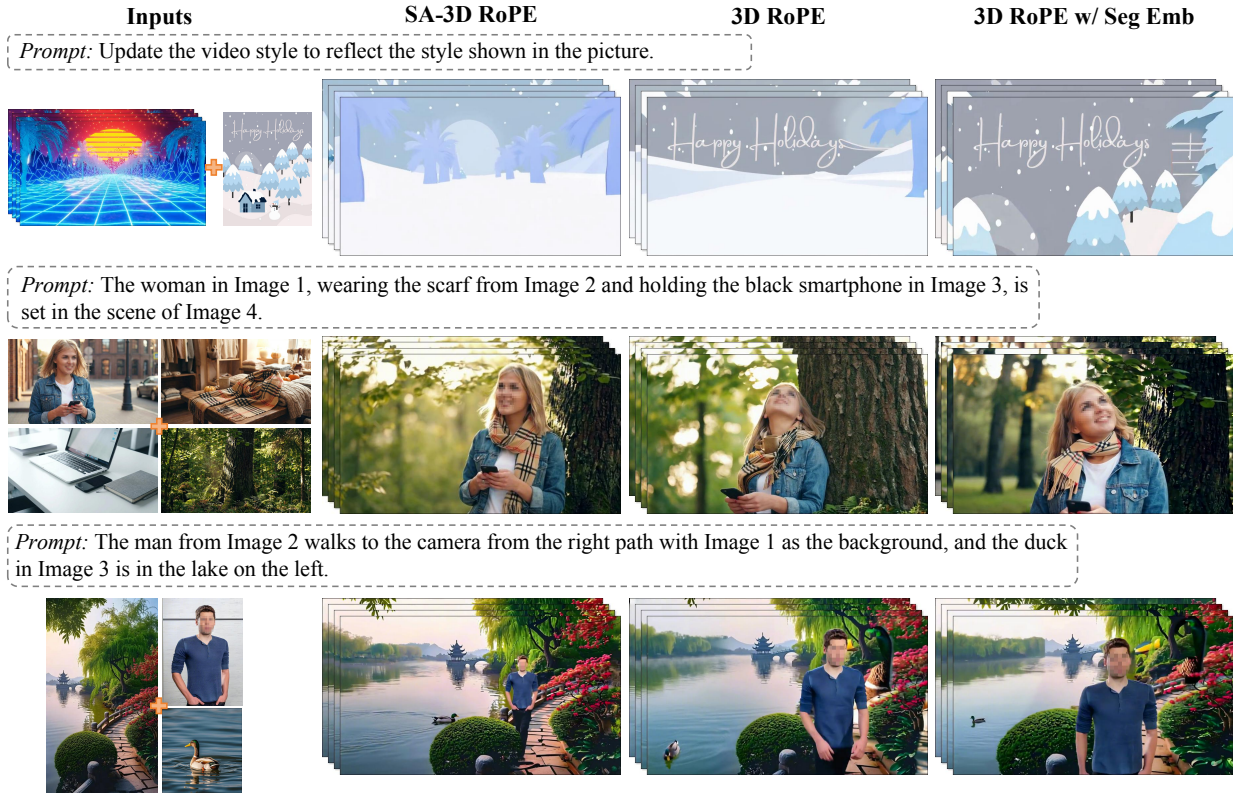


Figure 15 Ablation study of SA-3D RoPE, standard 3D RoPE and 3D RoPE with segment embedding on reference-guided video editing and subject-to-video tasks. Although incorporating segment embedding brings improvements in reference consistency (e.g., the scarf in the 2nd row), both baseline variants still suffer from noticeable reference leakage artifacts (e.g., the background in the 1st row and the duck head in the 3rd row).

Most notably, our approach attains a FaceSim score of **78.20**, exceeding the next-best baseline Kling O3 (57.20) by over 20 absolute points. This pronounced margin demonstrates substantially stronger face-identity preservation, which has long been a key bottleneck in multi-reference subject-driven video generation.

6.6 Ablation Studies

Effect of SA-3D RoPE. We further examine the contribution of segment-aware position encoding by comparing SA-3D RoPE against two baselines in reference-based video editing: the standard 3D RoPE, and the standard 3D RoPE with learnable segment embeddings. In this unified sequence, target tokens, source video tokens, and reference image tokens coexist. For the segment embedding baseline, segment embeddings are added to the hidden states at each DiT layer, utilizing the same segment IDs as SA-3D RoPE. As shown in Fig. 15, while the explicit segment embeddings improve reference consistency over the vanilla 3D RoPE, both baselines fail to cleanly isolate features. Consequently, they both suffer from content confusion, causing appearance details from the reference image to leak into unintended regions of the target. This confirms that additive segment embeddings are insufficient when multiple visual segments share the same (t, h, w) coordinates, the renderer cannot reliably distinguish their roles. SA-3D RoPE introduces a segment-index-conditioned phase modulation that decouples segment identity from spatiotemporal position, allowing attention to attend to the correct segment while preserving the original spatiotemporal modeling properties of 3D RoPE.

Effect of ViT Semantic Interface and MLLM Planner. As shown in Fig. 16, both the ViT embedding decoder and the MLLM planner are crucial for high-quality video editing. Our full model accurately performs object replacement and style transfer while preserving scene consistency. Removing the ViT semantic interface leads to weaker instruction following, such as failing to replace the robot with a robotic dog or omitting the flying

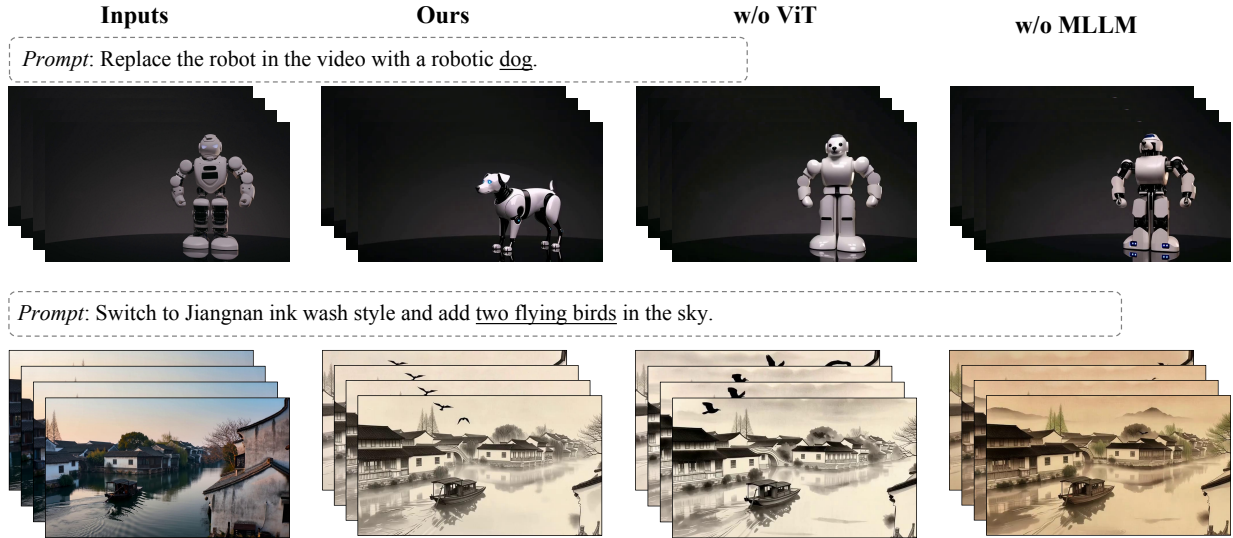


Figure 16 Ablation study on the ViT semantic interface and the MLLM planner.

birds in the Jiangnan ink wash style editing. Removing both ViT and MLLM further degrades the results, demonstrating their complementary roles in precise and faithful editing.

6.7 Generalizations

As shown in Figs. 17 and 18, Bernini demonstrates strong generalization to diverse video editing instructions. Benefiting from heterogeneous I2I and I2V training data, Bernini successfully transfers the learned instruction-following capability to video editing scenarios, including watercolor stylization, 2D/3D animation, weather changes, and effect additions, as illustrated in Fig. 17.

Furthermore, Bernini can handle editing instructions that are not explicitly present in the training data, such as motion changes, focus shifts, position changes, and causal reasoning, as shown in Fig. 18. Moreover, it supports reasoning-based editing: given the prompt about prolonged heavy rain, Bernini correctly infers that the fire should be extinguished, despite the absence of explicit causal supervision in the training data. These results suggest that Bernini does not merely memorize or fit standard training transformations, but instead learns a transferable and compositional instruction-following ability for video editing.

7 Related Work

Joint Multimodal Backbones. One line of work merges understanding and generation into a single backbone that processes text and visual tokens together over a unified sequence. Emu3 [73] embodies the simplest form of this idea, tokenizing text, images, and videos into a shared discrete vocabulary and training a single transformer from scratch with pure next-token prediction. Janus [79] retains the unified autoregressive backbone but decouples the visual encoders for understanding and generation into two separate pathways, using a SigLIP-style encoder for perception and a VQ tokenizer for synthesis. Other works hybridize the modeling objective across modalities: Show-o [82] couples autoregressive text modeling with discrete diffusion over image tokens within a single transformer, and HunyuanImage 3.0 [7] extends this hybrid to a Mixture-of-Experts decoder that performs next-token prediction for text alongside diffusion-based prediction for image tokens. BAGEL [15] adopts a Mixture-of-Transformer-Experts architecture in which separate understanding and generation experts interact through shared self-attention, paired with dual visual encoders that capture pixel- and semantic-level features. Lumina-DiMOO [83] replaces autoregressive prediction altogether with fully discrete masked diffusion as a single training objective over both modalities under a shared vocabulary.

MLLMs as Conditioners for Visual Generation. A second line of work keeps the MLLM and the diffusion model as separate components and lets the MLLM provide conditioning signals, with works differing primarily in

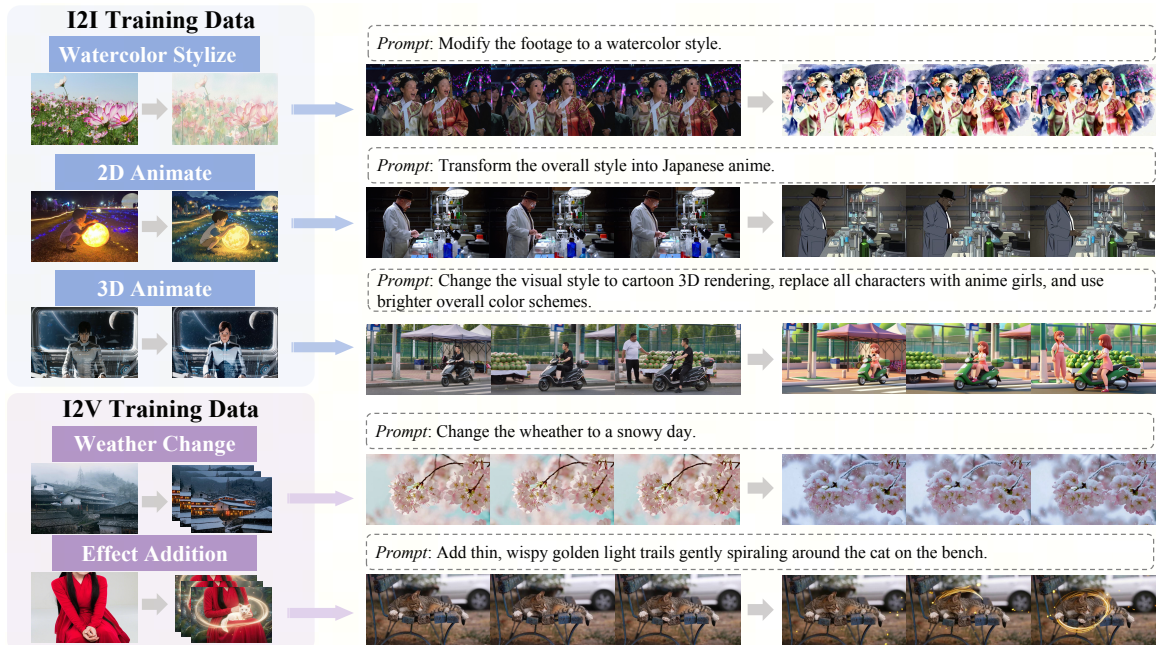


Figure 17 Video editing generalization through diverse I2I and I2V training data.

what representation carries the signal. The narrowest interfaces pass the MLLM’s output text tokens or a small group of learnable query tokens into the diffusion model through cross-attention: MetaQuery [54] and Bifrost-1 [42] fall into this category, with Bifrost-1 specifically using patch-level CLIP latents as the bridge. Wider interfaces use the MLLM’s hidden states directly: SEED-X [22], DreamLLM [18], and Emu [65] drive an external image decoder from these hidden states, while LaVi-Bridge [97] more broadly focuses on connecting frozen language and vision generators. The same hidden-state interface has been extended to video by UniVideo [76] and VInO [9], which couple an MLLM with a video diffusion backbone and feed MLLM hidden states (optionally augmented with learnable query tokens or interleaved multimodal context, alongside VAE latents of references) into the generator, unifying subject-to-video [16, 21, 31, 45, 72] and instruction-based editing [3, 26, 67, 81] under a single framework. Our work, Bernini, follows this decoupled paradigm but anchors the interface to the MLLM’s own ViT embedding space rather than its output hidden states, so that pretrained visual semantics can be transferred to the diffusion renderer at their native representation.

8 Conclusion and Limitations

We presented Bernini, a unified framework for video generation and editing that decouples semantic planning from pixel rendering: an MLLM planner predicts the target in its native ViT embedding space, and a DiT renderer synthesizes pixels conditioned on this plan, augmented by text and source VAE features. This interface lets the two components be trained largely independently while preserving their pretrained strengths. With SA-3D RoPE for multi-segment disambiguation and a latent chain-of-thought planner, Bernini achieves state-of-the-art results across video editing and subject-to-video benchmarks, and generalizes to challenging instructions beyond standard training cases.

Bernini remains much limited by our adopted foundation models for both MLLM planner and DiT renderer. In complex editing scenarios, it still depends on a strong LLM rewriter to provide sufficiently detailed and structured instructions, indicating that its native reasoning ability is not yet fully sufficient for challenging edits. In addition, while Bernini achieves state-of-the-art consistency in subject-to-video generation, its visual quality still falls short of stronger closed-source systems such as Wan2.7. More powerful foundation model instantiations could be helpful to further improve results.

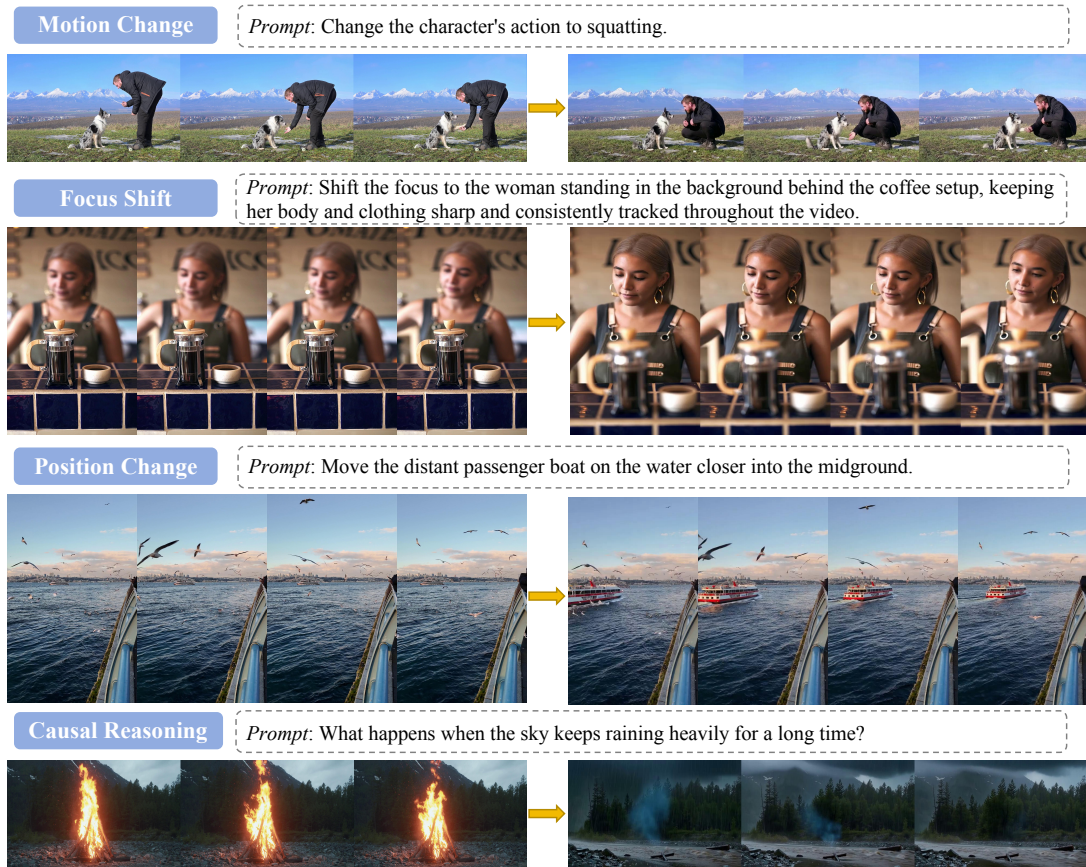


Figure 18 Generalization to diverse video editing instructions.

9 Contributions and Acknowledgements

Authors are organized by contribution role. All algorithm authors contributed equally to this work and are listed in alphabetical order by first name. † indicates the Project Lead.

Algorithm: Chenchen Liu, Junyi Chen, Lei Li, Lu Chi†, Mingzhen Sun, Zhuoying Li

Infrastructure: Yi Fu, Ruoyu Guo, Yiheng Wu, Ge Bai

Team Leader: Zehuan Yuan

We would like to thank Ruibiao Lu, Mingyang Zou and Zhen Ye for their support throughout this project.

References

- [1] Jianhong Bai, Menghan Xia, Xintao Wang, Ziyang Yuan, Xiao Fu, Zuozhu Liu, Haoji Hu, Pengfei Wan, and Di Zhang. Syncmaster: Synchronizing multi-camera video generation from diverse viewpoints. [arXiv preprint arXiv:2412.07760](#), 2024.
- [2] Jianhong Bai, Menghan Xia, Xiao Fu, Xintao Wang, Lianrui Mu, Jinwen Cao, Zuozhu Liu, Haoji Hu, Xiang Bai, Pengfei Wan, and Di Zhang. Recammaster: Camera-controlled generative rendering from a single video. In [Proceedings of the IEEE/CVF International Conference on Computer Vision \(ICCV\)](#), 2025.
- [3] Qingyan Bai, Qiuyu Wang, Hao Ouyang, Yue Yu, Hanlin Wang, Wen Wang, Ka Leong Cheng, Shuailei Ma, Yanhong Zeng, Zichen Liu, et al. Scaling instruction-based video editing with a high-quality synthetic dataset. [arXiv preprint arXiv:2510.15742](#), 2025.
- [4] Shuai Bai, Yuxuan Cai, Ruizhe Chen, Keqin Chen, Xionghui Chen, Zesen Cheng, Lianghao Deng, Wei Ding, Chang Gao, Chunjiang Ge, et al. Qwen3-vl technical report. [arXiv preprint arXiv:2511.21631](#), 2025.
- [5] Ralph Allan Bradley and Milton E. Terry. Rank analysis of incomplete block designs: I. the method of paired comparisons. [Biometrika](#), 39(3/4):324–345, 1952.
- [6] ByteDance. Jimeng AI. <https://jimeng.jianying.com>, 2024.
- [7] Siyu Cao, Hangting Chen, Peng Chen, Yiji Cheng, Yutao Cui, Xincheng Deng, Ying Dong, Kipper Gong, Tianpeng Gu, Xiuse Gu, et al. Hunyuanimage 3.0 technical report. [arXiv preprint arXiv:2509.23951](#), 2025.
- [8] Huiwen Chang, Han Zhang, Lu Jiang, Ce Liu, and William T Freeman. Maskgit: Masked generative image transformer. In [Proceedings of the IEEE/CVF Conference on Computer Vision and Pattern Recognition](#), pages 11315–11325, 2022.
- [9] Junyi Chen, Tong He, Zhoujie Fu, Pengfei Wan, Kun Gai, and Weicai Ye. VINO: A unified visual generator with interleaved omnimodal context. [arXiv preprint arXiv:2601.02358](#), 2026.
- [10] Junying Chen, Zhenyang Cai, Pengcheng Chen, Shunian Chen, Ke Ji, Xidong Wang, Yunjin Yang, and Benyou Wang. Sharegpt-4o-image: Aligning multimodal models with gpt-4o-level image generation. [arXiv preprint arXiv:2506.18095](#), 2025.
- [11] Zhe Chen, Jiannan Wu, Wenhai Wang, Weijie Su, Guo Chen, Sen Xing, Muyan Zhong, Qinglong Zhang, Xizhou Zhu, Lewei Lu, Bin Li, Ping Luo, Tong Lu, Yu Qiao, and Jifeng Dai. Intern VL: scaling up vision foundation models and aligning for generic visual-linguistic tasks. In [Proceedings of the IEEE/CVF Conference on Computer Vision and Pattern Recognition \(CVPR\)](#), 2024.
- [12] Jiaxin Cheng, Tianjun Xiao, and Tong He. Consistent video-to-video transfer using synthetic dataset. [arXiv preprint arXiv:2311.00213](#), 2023.
- [13] Yufeng Cui, Honghao Chen, Haoge Deng, Xu Huang, Xinghang Li, Jirong Liu, Yang Liu, Zhuoyan Luo, Jinsheng Wang, Wenxuan Wang, et al. Emu3. 5: Native multimodal models are world learners. [arXiv preprint arXiv:2510.26583](#), 2025.
- [14] Dao-AILab. Quack: A quirky assortment of cute kernels, 2025. URL <https://github.com/Dao-AILab/quack>. GitHub repository.
- [15] Chaorui Deng, Deyao Zhu, Kunchang Li, Chenhui Gou, Feng Li, Zeyu Wang, Shu Zhong, Weihao Yu, Xiaonan Nie, Ziang Song, Guang Shi, and Haoqi Fan. Emerging properties in unified multimodal pretraining. [arXiv preprint arXiv:2505.14683](#), 2025.
- [16] Yufan Deng, Xun Guo, Shenghai Yuan, Zhaoxi Chen, Peng Zhou, Tianyu Ma, Boyuan Chen, Bin Lin, Li Yuan, and Wanli Wang. Magref: Masked guidance for any-reference video generation with subject disentanglement. [arXiv preprint arXiv:2505.23742](#), 2025.
- [17] Juechu Dong, Boyuan Feng, Driss Guessous, Yanbo Liang, and Horace He. Flex attention: A programming model for generating optimized attention kernels. [arXiv preprint arXiv:2412.05496](#), 2(3):4, 2024.
- [18] Runpei Dong, Chunrui Han, Yuang Peng, Zekun Qi, Zheng Ge, Jinrong Yang, Liang Zhao, Jianjian Sun, Hongyu Zhou, Haoran Wei, Xiangwen Kong, Xiangyu Zhang, Kaisheng Ma, and Li Yi. Dreamllm: Synergistic multimodal comprehension and creation. 2024.

- [19] Alexey Dosovitskiy, Lucas Beyer, Alexander Kolesnikov, Dirk Weissenborn, Xiaohua Zhai, Thomas Unterthiner, Mostafa Dehghani, Matthias Minderer, Georg Heigold, Sylvain Gelly, Jakob Uszkoreit, and Neil Houlsby. An image is worth 16x16 words: Transformers for image recognition at scale. In International Conference on Learning Representations (ICLR), 2021.
- [20] Patrick Esser, Sumith Kulal, Andreas Blattmann, Rahim Entezari, Jonas Müller, Harry Saini, Yam Levi, Dominik Lorenz, Axel Sauer, Frederic Boesel, Dustin Podell, Tim Dockhorn, Zion English, and Robin Rombach. Scaling rectified flow transformers for high-resolution image synthesis. 2024.
- [21] Zhengcong Fei, Debang Li, Di Qiu, Jiahua Yu, and Mingyuan Fan. Skyreels-a2: Compose anything in video diffusion transformers. arXiv preprint arXiv:2504.02436, 2025.
- [22] Yuying Ge, Sijie Zhao, Jinguo Zhu, Yixiao Ge, Kun Yi, Lin Song, Chen Li, Xiaohan Ding, and Ying Shan. Seed-x: Multimodal models with unified multi-granularity comprehension and generation. arXiv preprint arXiv:2404.14396, 2024.
- [23] Michal Geyer, Omer Bar-Tal, Shai Bagon, and Tali Dekel. Tokenflow: Consistent diffusion features for consistent video editing. In International Conference on Learning Representations (ICLR), 2024.
- [24] Google DeepMind. Veo 3. <https://deepmind.google/models/veo/>, 2025.
- [25] Feng Han, Yibin Wang, Chenglin Li, Zheming Liang, Dianyi Wang, Yang Jiao, Zhipeng Wei, Chao Gong, Cheng Jin, Jingjing Chen, et al. Unireditbench: A unified reasoning-based image editing benchmark. arXiv preprint arXiv:2511.01295, 2025.
- [26] Haoyang He, Jie Wang, Jiangning Zhang, Zhucun Xue, Xingyuan Bu, Qiangpeng Yang, Shilei Wen, and Lei Xie. Openve-3m: A large-scale high-quality dataset for instruction-guided video editing. arXiv preprint arXiv:2512.07826, 2025.
- [27] Zhihao He, Tiejun Chen, Kangyu Wang, Ziran Qin, Yang Shao, Chaofan Gan, Shijie Li, Zuxuan Wu, and Weiyao Lin. Vidlada: Bidirectional diffusion large language models for efficient video understanding. arXiv preprint arXiv:2601.17868, 2026.
- [28] Yushi Hu, Weijia Shi, Xingyu Fu, Dan Roth, Mari Ostendorf, Luke Zettlemoyer, Noah A Smith, and Ranjay Krishna. Visual sketchpad: Sketching as a visual chain of thought for multimodal language models. In Advances in Neural Information Processing Systems (NeurIPS), 2024.
- [29] Ziqi Huang, Yinan He, Jiashuo Yu, Fan Zhang, Chenyang Si, Yuming Jiang, Yuanhan Zhang, Tianxing Wu, Qingyang Jin, Nattapol Chanpaisit, Yaohui Wang, Xinyuan Chen, Limin Wang, Dahua Lin, Yu Qiao, and Ziwei Liu. VBench: Comprehensive benchmark suite for video generative models. In Proceedings of the IEEE/CVF Conference on Computer Vision and Pattern Recognition (CVPR), 2024.
- [30] Sam Ade Jacobs, Masahiro Tanaka, Chengming Zhang, Minjia Zhang, Shuaiwen Leon Song, Samyam Rajbhandari, and Yuxiong He. DeepSpeed Ulysses: System optimizations for enabling training of extreme long sequence transformer models, 2023. URL <https://arxiv.org/abs/2309.14509>.
- [31] Zeyinzi Jiang, Zhen Han, Chaojie Mao, Jingfeng Zhang, Yulin Pan, and Yu Liu. Vace: All-in-one video creation and editing. In Proceedings of the IEEE/CVF International Conference on Computer Vision, pages 17191–17202, 2025.
- [32] Xuan Ju, Tianyu Wang, Yuqian Zhou, He Zhang, Qing Liu, Nanxuan Zhao, Zhifei Zhang, Yijun Li, Yuanhao Cai, Shaoteng Liu, et al. Editverse: Unifying image and video editing and generation with in-context learning. arXiv preprint arXiv:2509.20360, 2025.
- [33] Weijie Kong, Qi Tian, Zijian Zhang, Rox Min, Zuozhuo Dai, Jin Zhou, Jiangfeng Xiong, Xin Li, Bo Wu, Jianwei Zhang, et al. HunyuanVideo: A systematic framework for large video generative models. arXiv preprint arXiv:2412.03603, 2024.
- [34] Kuaishou Technology. Kling 1.6. <https://klingai.com/>, 2024. Accessed: 2026-04-22.
- [35] Maksim Kuprashevich, Grigorii Alekseenko, Irina Tolstykh, Georgii Fedorov, Bulat Suleimanov, Vladimir Dokholyan, and Aleksandr Gordeev. Nohumansrequired: Autonomous high-quality image editing triplet mining. arXiv preprint arXiv:2507.14119, 2025.
- [36] Black Forest Labs. FLUX.1. <https://blackforestlabs.ai/>, 2024.

- [37] Minghan Li, Chenxi Xie, Yichen Wu, Lei Zhang, and Mengyu Wang. Five: A fine-grained video editing benchmark for evaluating emerging diffusion and rectified flow models. [arXiv preprint arXiv:2503.13684](#), 2025.
- [38] Qingyun Li, Zhe Chen, Weiyun Wang, Wenhai Wang, Shenglong Ye, Zhenjiang Jin, Guanzhou Chen, Yinan He, Zhangwei Gao, Erfei Cui, et al. Omnicorpus: A unified multimodal corpus of 10 billion-level images interleaved with text. [arXiv preprint arXiv:2406.08418](#), 2024.
- [39] Tianhong Li, Yonglong Tian, He Li, Mingyang Deng, and Kaiming He. Autoregressive image generation without vector quantization. *Advances in Neural Information Processing Systems*, 37:56424–56445, 2024.
- [40] Xiaowen Li, Haolan Xue, Peiran Ren, and Liefeng Bo. Diffueraser: A diffusion model for video inpainting. [arXiv preprint arXiv:2501.10018](#), 2025.
- [41] Xinyao Liao, Xianfang Zeng, Ziyi Song, Zhoujie Fu, Gang Yu, and Guosheng Lin. In-context learning with unpaired clips for instruction-based video editing. [arXiv preprint arXiv:2510.14648](#), 2025.
- [42] Han Lin, Jaemin Cho, Amir Zadeh, Chuan Li, and Mohit Bansal. Bifrost-1: Bridging multimodal llms and diffusion models with patch-level CLIP latents. [arXiv preprint arXiv:2508.05954](#), 2025.
- [43] Yaron Lipman, Ricky T. Q. Chen, Heli Ben-Hamu, Maximilian Nickel, and Matt Le. Flow matching for generative modeling. [arXiv preprint arXiv:2210.02747](#), 2022.
- [44] Haotian Liu, Chunyuan Li, Qingyang Wu, and Yong Jae Lee. Visual instruction tuning. [arXiv preprint arXiv:2304.08485](#), 2023.
- [45] Lijie Liu, Tianxiang Liu, Zhichao Wang, Yubin Zhao, Jun Chen, Zhongyuan Zhang, Boyuan Gong, and Jiashi Deng. Phantom: Subject-consistent video generation via cross-modal alignment. [arXiv preprint arXiv:2502.11079](#), 2025.
- [46] Shilong Liu, Zhaoyang Zeng, Tianhe Ren, Feng Li, Hao Zhang, Jie Yang, Chunyuan Li, Jianwei Yang, Hang Su, Jun Zhu, et al. Grounding dino: Marrying dino with grounded pre-training for open-set object detection. [arXiv preprint arXiv:2303.05499](#), 2023.
- [47] Kingchao Liu, Chengyue Gong, and Qiang Liu. Flow straight and fast: Learning to generate and transfer data with rectified flow, 2022. URL <https://arxiv.org/abs/2209.03003>.
- [48] Yawen Luo, Xiaoyu Shi, Jianhong Bai, Menghan Xia, Tianfan Xue, Xintao Wang, Pengfei Wan, Di Zhang, and Kun Gai. Camclonemaster: Enabling reference-based camera control for video generation. In *Proceedings of the SIGGRAPH Asia 2025 Conference Papers*, pages 1–10, 2025.
- [49] Guoqing Ma, Haoyang Huang, Kun Yan, Liangyu Chen, Nan Duan, Shengming Yin, Changyi Guo, Junshu Huang, Zhenyu Liu, Weihong Zhang, et al. Step-Video-T2V technical report: The practice, challenges, and future of video foundation model. [arXiv preprint arXiv:2502.10248](#), 2025.
- [50] Yiwei Ma, Guohai Xu, Xiaoshuai Sun, Ming Yan, Ji Zhang, and Rongrong Ji. X-clip: End-to-end multi-grained contrastive learning for video-text retrieval. In *Proceedings of the 30th ACM international conference on multimedia*, pages 638–647, 2022.
- [51] Chenlin Meng, Robin Rombach, Ruiqi Gao, Diederik P Kingma, Stefano Ermon, Jonathan Ho, and Tim Salimans. On distillation of guided diffusion models. In *CVPR*, 2023.
- [52] Antoine Miech, Dimitri Zhukov, Jean-Baptiste Alayrac, Makarand Tapaswi, Ivan Laptev, and Josef Sivic. Howto100m: Learning a text-video embedding by watching hundred million narrated video clips. In *Proceedings of the IEEE/CVF international conference on computer vision*, pages 2630–2640, 2019.
- [53] OpenAI. Sora: Creating video from text. <https://openai.com/sora>, 2024.
- [54] Xichen Pan, Satya Narayan Shukla, Aashu Singh, Zhuokai Zhao, Shlok Kumar Mishra, Jialiang Wang, Zhiyang Xu, Jiuhai Chen, Kungpeng Li, Felix Juefei-Xu, Ji Hou, and Saining Xie. Transfer between modalities with metaqueries. [arXiv preprint arXiv:2504.06256](#), 2025.
- [55] William Peebles and Saining Xie. Scalable diffusion models with transformers. In *Proceedings of the IEEE/CVF International Conference on Computer Vision (ICCV)*, 2023.
- [56] Pika Labs. Pika 2.1. <https://pika.art/>, 2024. Accessed: 2026-04-22.

- [57] Yusu Qian, Eli Bocek-Rivele, Liangchen Song, Jialing Tong, Yinfei Yang, Jiasen Lu, Wenzhe Hu, and Zhe Gan. Pico-banana-400k: A large-scale dataset for text-guided image editing. [arXiv preprint arXiv:2510.19808](#), 2025.
- [58] Alec Radford, Jong Wook Kim, Chris Hallacy, Aditya Ramesh, Gabriel Goh, Sandhini Agarwal, Girish Sastry, Amanda Askell, Pamela Mishkin, Jack Clark, et al. Learning transferable visual models from natural language supervision. In [International conference on machine learning](#), pages 8748–8763. PmLR, 2021.
- [59] Nikhila Ravi, Valentin Gabeur, Yuan-Ting Hu, Ronghang Hu, Chaitanya Ryali, Tengyu Ma, Haitham Khedr, Roman Rädle, Chloe Rolland, Laura Gustafson, Eric Mintun, Junting Pan, Kalyan Vasudev Alwala, Nicolas Carion, Chao-Yuan Wu, Ross Girshick, Piotr Dollár, and Christoph Feichtenhofer. Sam 2: Segment anything in images and videos, 2024. URL <https://arxiv.org/abs/2408.00714>.
- [60] Robin Rombach, Andreas Blattmann, Dominik Lorenz, Patrick Esser, and Björn Ommer. High-resolution image synthesis with latent diffusion models. In [Proceedings of the IEEE/CVF Conference on Computer Vision and Pattern Recognition \(CVPR\)](#), 2022.
- [61] Runway. Introducing Gen-3 Alpha: A new frontier for video generation. <https://runwayml.com/research/introducing-gen-3-alpha>, 2024.
- [62] Seyedmorteza Sadat, Otmar Hilliges, and Romann M Weber. Eliminating oversaturation and artifacts of high guidance scales in diffusion models. In [The Thirteenth International Conference on Learning Representations](#), 2024.
- [63] Shengshu Technology. Vidu 2.0. <https://www.vidu.com/>, 2024. Accessed: 2026-04-22.
- [64] Jianlin Su, Yu Lu, Shengfeng Pan, Bo Wen, and Yunfeng Liu. RoFormer: Enhanced transformer with rotary position embedding. [arXiv preprint arXiv:2104.09864](#), 2021.
- [65] Quan Sun, Qiying Yu, Yufeng Cui, Fan Zhang, Xiaosong Zhang, Yueze Wang, Hongcheng Gao, Jingjing Liu, Tiejun Huang, and Xinlong Wang. Emu: Generative pretraining in multimodality. [arXiv preprint arXiv:2307.05222](#), 2023.
- [66] Zhiyu Tan, Hao Yang, Luozheng Qin, Jia Gong, Mengping Yang, and Hao Li. Omni-video: Democratizing unified video understanding and generation. [arXiv preprint arXiv:2507.06119](#), 2025.
- [67] DecartAI Team. Lucy edit: Open-weight text-guided video editing. 2025. URL https://d2drjpuinn461b.cloudfront.net/Lucy_Edit_High_Fidelity_Text_Guided_Video_Editing.pdf.
- [68] Kling Team, Jialu Chen, Yuanzheng Ci, Xiangyu Du, Zipeng Feng, Kun Gai, Sainan Guo, Feng Han, Jingbin He, Kang He, et al. Kling-omni technical report. [arXiv preprint arXiv:2512.16776](#), 2025.
- [69] Qwen Team. Qwen2.5-vl technical report. [arXiv preprint arXiv:2502.13923](#), 2025.
- [70] Wan Team. Wan: Open and advanced large-scale video generative models. [arXiv preprint arXiv:2503.20314](#), 2025.
- [71] Michael Tschanen, Alexey Gritsenko, Xiao Wang, Muhammad Ferjad Naeem, Ibrahim Alabdulmohsin, Nikhil Parthasarathy, Talfan Evans, Lucas Beyer, Ye Xia, Basil Mustafa, Olivier Hénaff, Jeremiah Harmsen, Andreas Steiner, and Xiaohua Zhai. SigLIP 2: Multilingual vision-language encoders with improved semantic understanding, localization, and dense features. [arXiv preprint arXiv:2502.14786](#), 2025.
- [72] Lei Wang, Yuxin Song, Ge Wu, Haocheng Feng, Hang Zhou, Jingdong Wang, Yaxing Wang, and Jian Yang. Refalign: Representation alignment for reference-to-video generation. [arXiv preprint arXiv:2603.25743](#), 2026.
- [73] Xinlong Wang, Xiaosong Zhang, Zhengxiong Luo, Quan Sun, Yufeng Cui, Jinsheng Wang, Fan Zhang, Yueze Wang, Zhen Li, Qiying Yu, Yingli Zhao, Yulong Ao, Xuebin Min, Tao Li, Boya Wu, Bo Zhao, Bowen Zhang, Liangdong Wang, Guang Liu, Zheqi He, Xi Yang, Jingjing Liu, Yonghua Lin, Tiejun Huang, and Zhongyuan Wang. Emu3: Next-token prediction is all you need. [arXiv preprint arXiv:2409.18869](#), 2024.
- [74] Yuhan Wang, Siwei Yang, Bingchen Wang, Letian Tu, Bingyu Li, Yuyin Hong, Yibing Wang, Yuyou Yan, Alan Yuille, and Cihang Xie. Gpt-image-edit-1.5m: A million-scale, gpt-generated image dataset. [arXiv preprint arXiv:2507.21033](#), 2025.
- [75] Cong Wei, Zheyang Xiong, Weiming Ren, Xeron Du, Ge Zhang, and Wenhui Chen. Omniedit: Building image editing generalist models through specialist supervision. In [The Thirteenth International Conference on Learning Representations](#), 2024.

- [76] Cong Wei, Quande Liu, Zixuan Ye, Qiulin Wang, Xintao Wang, Pengfei Wan, Kun Gai, and Wenhui Chen. Univideo: Unified video understanding, generation, and editing. [arXiv preprint arXiv:2510.08377](#), 2026.
- [77] Jason Wei, Xuezhi Wang, Dale Schuurmans, Maarten Bosma, Brian Ichter, Fei Xia, Ed Chi, Quoc Le, and Denny Zhou. Chain-of-thought prompting elicits reasoning in large language models. 2022.
- [78] Luis Wiedmann, Orr Zohar, Amir Mahla, Xiaohan Wang, Rui Li, Thibaud Frere, Leandro von Werra, Aritra Roy Gosthipaty, and Andrés Marafioti. Finevision: Open data is all you need. [arXiv preprint arXiv:2510.17269](#), 2025.
- [79] Chengyue Wu, Xiaokang Chen, Zhiyu Wu, Yiyang Ma, Xingchao Liu, Zizheng Pan, Wen Liu, Zhenda Xie, Xingkai Yu, Chong Ruan, and Ping Luo. Janus: Decoupling visual encoding for unified multimodal understanding and generation. In [Proceedings of the IEEE/CVF Conference on Computer Vision and Pattern Recognition \(CVPR\)](#), 2025.
- [80] Chenyuan Wu, Pengfei Zheng, Ruiran Yan, Shitao Xiao, Xin Luo, Yuezhe Wang, Wanli Li, Xiyan Jiang, Yexin Liu, Junjie Zhou, Ze Liu, Ziyi Xia, Chaofan Li, Haoge Deng, Jiahao Wang, Kun Luo, Bo Zhang, Defu Lian, Xinlong Wang, Zhongyuan Wang, Tiejun Huang, and Zheng Liu. Omnigen2: Exploration to advanced multimodal generation. 2025.
- [81] Yuhui Wu, Liyi Chen, Ruibin Li, Shihao Wang, Chenxi Xie, and Lei Zhang. Insvie-1m: Effective instruction-based video editing with elaborate dataset construction. In [Proceedings of the IEEE/CVF International Conference on Computer Vision](#), pages 16692–16701, 2025.
- [82] Jinheng Xie, Weijia Mao, Zechen Bai, David Junhao Zhang, Weihao Wang, Kevin Qinghong Lin, Yuchao Gu, Zhijie Chen, Zhenheng Yang, and Mike Zheng Shou. Show-o: One single transformer to unify multimodal understanding and generation. [arXiv preprint arXiv:2408.12528](#), 2024.
- [83] Yi Xin, Qi Qin, Siqi Luo, Kaiwen Zhu, Juncheng Yan, Yan Tai, Jiayi Lei, Yuewen Cao, Keqi Wang, Yibin Wang, Jinbin Bai, Qian Yu, Dengyang Jiang, Yuandong Pu, Haoxing Chen, Le Zhuo, Junjun He, Gen Luo, Tianbin Li, Ming Hu, Jin Ye, Shenglong Ye, Bo Zhang, Chang Xu, Wenhai Wang, Hongsheng Li, Guangtao Zhai, Tianfan Xue, Bin Fu, Xiaohong Liu, Yu Qiao, and Yihao Liu. Lumina-dimoo: An omni diffusion large language model for multi-modal generation and understanding. [arXiv preprint arXiv:2510.06308](#), 2025.
- [84] An Yang, Anfeng Li, Baosong Yang, Beichen Zhang, Binyuan Hui, Bo Zheng, Bowen Yu, Chang Gao, Chengen Huang, Chenxu Lv, et al. Qwen3 technical report. [arXiv preprint arXiv:2505.09388](#), 2025.
- [85] Zhendong Yang, Ailing Zeng, Chun Yuan, and Yu Li. Effective whole-body pose estimation with two-stages distillation. In [Proceedings of the IEEE/CVF International Conference on Computer Vision](#), pages 4210–4220, 2023.
- [86] Zhuoyi Yang, Jiayan Teng, Wendi Zheng, Ming Ding, Shiyu Huang, Jiazheng Xu, Yuanming Yang, Wenyi Hong, Xiaohan Zhang, Guanyu Feng, Da Yin, Xiaotao Gu, Yuxuan Zhang, Weihao Wang, Yean Cheng, Ting Liu, Bin Xu, Yuxiao Dong, and Jie Tang. CogVideoX: Text-to-video diffusion models with an expert transformer. In [International Conference on Learning Representations \(ICLR\)](#), 2025.
- [87] Danah Yatim, Rafail Fridman, Omer Bar-Tal, Yoni Kasten, and Tali Dekel. Space-time diffusion features for zero-shot text-driven motion transfer. In [Proceedings of the IEEE/CVF Conference on Computer Vision and Pattern Recognition \(CVPR\)](#), pages 8466–8476, 2024.
- [88] Yang Ye, Xianyi He, Zongjian Li, Bin Lin, Shenghai Yuan, Zhiyuan Yan, Bohan Hou, and Li Yuan. Imgedit: A unified image editing dataset and benchmark. [arXiv preprint arXiv:2505.20275](#), 2025.
- [89] Mark Yu, Wenbo Hu, Jinbo Xing, and Ying Shan. Trajectorycrafter: Redirecting camera trajectory for monocular videos via diffusion models. In [Proceedings of the IEEE/CVF international conference on computer vision](#), pages 100–111, 2025.
- [90] Qifan Yu, Wei Chow, Zhongqi Yue, Kaihang Pan, Yang Wu, Xiaoyang Wan, Juncheng Li, Siliang Tang, Hanwang Zhang, and Yueting Zhuang. Anyedit: Mastering unified high-quality image editing for any idea. In [Proceedings of the IEEE/CVF Conference on Computer Vision and Pattern Recognition \(CVPR\)](#), 2025.
- [91] Shenghai Yuan, Xianyi He, Yufan Deng, Yang Ye, Jinfa Huang, Bin Lin, Jiebo Luo, and Li Yuan. Opens2v-nexus: A detailed benchmark and million-scale dataset for subject-to-video generation. [arXiv preprint arXiv:2505.20292](#), 2025.

- [92] Ted Zadouri, Markus Hoehnerbach, Jay Shah, Timmy Liu, Vijay Thakkar, and Tri Dao. Flashattention-4: Algorithm and kernel pipelining co-design for asymmetric hardware scaling. [arXiv preprint arXiv:2603.05451](#), 2026.
- [93] Kai Zhang, Lingbo Mo, Wenhui Chen, Huan Sun, and Yu Su. Magicbrush: A manually annotated dataset for instruction-guided image editing. In [Advances in Neural Information Processing Systems](#), 2023.
- [94] Yifu Zhang, Hao Yang, Yuqi Zhang, Yifei Hu, Fengda Zhu, Chuang Lin, Xiaofeng Mei, Yi Jiang, Bingyue Peng, and Zehuan Yuan. Waver: Wave your way to lifelike video generation. [arXiv preprint arXiv:2508.15761](#), 2025.
- [95] Yuanhan Zhang, Jinming Wu, Wei Li, Bo Li, Zejun Ma, Ziwei Liu, and Chunyuan Li. Llava-video: Video instruction tuning with synthetic data. [arXiv preprint arXiv:2410.02713](#), 2024.
- [96] Haozhe Zhao, Xiaojian Ma, Liang Chen, Shuzheng Si, Rujie Wu, Kaikai An, Peiyu Yu, Minjia Zhang, Qing Li, and Baobao Chang. Ultraedit: Instruction-based fine-grained image editing at scale. [Advances in Neural Information Processing Systems](#), 2024.
- [97] Shihao Zhao, Shaozhe Hao, Bojia Zi, Huaizhe Xu, and Kwan-Yee K. Wong. Bridging different language models and generative vision models for text-to-image generation. 2024.
- [98] Zijian Zhou, Shikun Liu, Haozhe Liu, Haonan Qiu, Zhaochong An, Weiming Ren, Zhiheng Liu, Xiaoke Huang, Kam Woh Ng, Tian Xie, Xiao Han, Yuren Cong, Hang Li, Chuyan Zhu, Aditya Patel, Tao Xiang, and Sen He. Scaling zero-shot reference-to-video generation. [arXiv preprint](#), 2025.
- [99] Bojia Zi et al. Señorita-2m: A high-quality instruction-based dataset for general video editing by video specialists. In [Advances in Neural Information Processing Systems \(NeurIPS\)](#), 2025.

Appendix

A MLLM Prompts for Bernini-Bench Evaluation

You are a professional data rater specializing in evaluating instruction-driven video editing results. You will be given two videos (the original video before editing and the result video after editing) along with the corresponding editing instruction. Your task is to evaluate the editing quality on a 1-5 scale across four dimensions: Instruction Compliance, Video Consistency, Generation Quality, and Overall Performance.

Dimension 1 Instruction Compliance

Evaluate whether the editing instruction has been faithfully and completely executed. Focus on: Was the correct target edited? Is the action type correct (add / remove / replace / style transfer / background change / camera change, etc.)? Are all specified attributes (object class, count, position, colour, size, style, etc.) satisfied?

Special rule - "Non-execution": If the target video shows NO meaningful change from the original (minor colour shifts on non-colour instructions, or trivial changes in non-target areas do NOT count as execution), treat it as instruction non-compliance and score 1.

1 - Non-execution or completely wrong: The edited video shows NO meaningful change from the original video (instruction completely ignored, or the video is an identical copy; minor colour shifts on non-colour instructions or trivial irrelevant fluctuations do NOT count as execution), OR the video is corrupted / the edit is entirely wrong (wrong target, wrong action type, entirely unrelated change, or the foreground/background is destroyed in a way that has nothing to do with the instruction).

2 - The edit partially attempts the instruction but fundamentally fails: only a few frames are affected, the wrong object/class is edited, the action is applied to the wrong region, or the instruction is executed in a clearly incorrect way (e.g., object added on the wrong side, wrong style applied).

3 - The core instruction is largely followed (correct target, correct action type), but with significant errors: key attributes are wrong (e.g., count, position, colour clearly deviate from the prompt), remnants of removed objects remain, unintended objects are also edited, or the effect is highly inconsistent across frames.

4 - The instruction is correctly and fully executed for the entire duration. Only minor attribute inaccuracies remain (e.g., slight colour or size mismatch, minor position offset). All and only the intended targets are affected.

5 - Perfect execution: every aspect of the instruction is faithfully reproduced - target, action, class, number, position, scale, pose, motion, style, and detail all exactly match the prompt throughout the entire video.

Dimension 2 Video Consistency

Evaluate whether non-edited regions and editing-irrelevant attributes remain consistent before and after editing. This includes: background preservation, art style / colour tone consistency, subject identity consistency (same person, same object), spatial layout and geometry preservation, and motion continuity.

Important: Changes that are a NECESSARY and EXPECTED consequence of the editing instruction itself should NOT be penalised in this dimension (e.g., a camera shot change naturally alters the visible background; a style transfer naturally changes the colour palette). Only evaluate unintended or unnecessary deviations.

1 - The original scene is barely recognisable: background is completely replaced or destroyed, subject identity is lost, spatial layout is severely distorted, or art style is drastically and unnecessarily altered.

- 2 - The main subject is recognisable, but major unintended changes are present: background is significantly altered, subject's key features (shape, appearance, identity) are clearly different, or the overall colour tone / art style shifted noticeably without instruction.
- 3 - Overall structure and subject identity are maintained, but noticeable unintended deviations exist: moderate background changes, minor subject appearance drift (e.g., clothing colour shift, slight shape change), or mild art style inconsistency in some frames.
- 4 - Nearly all non-edited regions and attributes are well preserved. Only very minor, hard-to-spot deviations (e.g., subtle texture change in a small background area, very slight colour tone shift) that do not affect the overall viewing experience.
- 5 - Perfect preservation: all non-edited regions, subject identity, background, art style, spatial layout, and motion are completely unchanged. The edit is perfectly isolated to the instructed target.

Dimension 3 Generation Quality

Evaluate the visual quality, temporal stability, and physical plausibility of the edited video. Focus on: AI artifacts (pasting feel, unnatural blending, distortion, deformation), temporal coherence (flickering, jittering, "boiling" textures, frame discontinuity), seamlessness of integration (edges, colour/resolution matching, lighting/shadow consistency), and physical realism (correct perspective, shadows, reflections, occlusion, natural motion).

- 1 - Severe quality issues: extreme flickering or "boiling" effects, heavy distortion/deformation of generated content, obvious pasting feel with clear seams, or physically impossible results (floating objects, completely wrong perspective/lighting). The video is essentially unwatchable.
- 2 - Significant and distracting quality problems: obvious AI artifacts, strong temporal inconsistency (style flickers on/off, jittering edges), clear resolution/colour mismatch between edited and unedited regions, or major physical implausibilities (missing/static shadows, wrong occlusion).
- 3 - Noticeable but tolerable issues: moderate AI feel (slightly unnatural blending), some flickering or texture instability during motion, minor edge artefacts or colour bleeding, or small physical inconsistencies (slightly off shadows or perspective). The video is watchable but the edit is clearly visible upon normal viewing.
- 4 - Good quality with only minor issues: very slight AI artifacts visible only upon close inspection, largely stable with only subtle flickering in complex motion areas, well-matched lighting and colour, and believable physical interactions. Casual viewers would not notice the edit.
- 5 - Flawless quality: perfectly stable and temporally coherent with zero flickering, completely seamless integration indistinguishable from the original footage, physically correct lighting/shadows/reflections/perspective throughout, and natural motion. The edit appears as if it were part of the original recording.

Dimension 4 Overall Performance

Provide a holistic assessment: considering all the above dimensions together, how well does the edited video meet the user's likely expectation? This score reflects the overall subjective satisfaction - whether the result would be accepted by a real user as a successful edit.

- 1 - Completely fails to meet user expectations. The edit is unusable.
- 2 - The edit attempt is recognisable but the result is clearly unacceptable due to combined failures in compliance, consistency, or quality.
- 3 - A partially successful edit: the intent is understood and partially achieved, but noticeable issues in one or more dimensions reduce the result's usability.
- 4 - A good edit that would satisfy most users. Minor imperfections exist but do not significantly detract from the overall result.
- 5 - An excellent edit that fully meets or exceeds user expectations. The result is professional-grade and virtually indistinguishable from a manually crafted or real video.

Scoring Constraints

- If the instruction is not executed at all (non-execution), Instruction Compliance should be scored 1, and Video Consistency and Generation Quality should be skipped (marked as "N/A"). Overall Performance should be 1.

Response Format

Please output a valid JSON object exactly matching the following structure, without any extra markdown formatting or conversational text:

```
{  
  "Brief reasoning": "<A concise explanation covering all four dimensions, no more than 50 words.>",  
  
  "Instruction Compliance": "<1-5>",  
  "Video Consistency": "<1-5 or \"N/A\">",  
  "Generation Quality": "<1-5 or \"N/A\">",  
  "Overall Performance": "<1-5>"  
}
```

editing instruction is: {edit_prompt}.

Below are the videos before and after editing:

Prompt 1. Bernini-V2V evaluation prompt

You are a professional data rater specializing in evaluating reference-guided video editing results. You will be given an original video (before editing), a reference image (the visual exemplar that the edit should follow), the result video (after editing), and the corresponding editing instruction. Your task is to evaluate the editing quality on a 1-5 scale across five dimensions: Instruction Compliance, Video Consistency, Reference Image Consistency, Generation Quality, and Overall Performance.

Dimension 1 Instruction Compliance

Evaluate whether the editing instruction has been faithfully and completely executed, INDEPENDENT of the reference image. Focus purely on whether the correct action was performed on the correct target: Was the right object/region edited? Is the action type correct (add / remove / replace / change background / change style, etc.)? Are positional and structural requirements satisfied?

Note: The degree to which the result matches the reference image's appearance is evaluated separately in Dimension 3. Here, only evaluate the structural and semantic correctness of the editing action itself.

Special rule - "Non-execution": If the target video shows NO meaningful change from the original (minor colour shifts on non-colour instructions, or trivial changes in non-target areas do NOT count as execution), treat it as instruction non-compliance and score 1.

1 - Non-execution or completely wrong: The edited video shows NO meaningful change from the original video (instruction completely ignored, or the video is an identical copy; minor colour shifts on non-colour instructions or trivial irrelevant fluctuations do NOT count as execution), OR the video is corrupted / the edit is entirely wrong (wrong target, wrong action type, entirely unrelated change, or the foreground/background is destroyed in a way that has nothing to do with the instruction).

2 - The edit partially attempts the instruction but fundamentally fails: only a few frames are affected, the wrong object/class is edited, the action is applied to the wrong region, or the instruction is executed in a clearly incorrect way (e.g., object added on the wrong side, wrong style applied).

3 - The core instruction is largely followed (correct target, correct action type), but with significant errors: key attributes are wrong (e.g., count, position, colour clearly deviate from the prompt), remnants of removed objects remain, unintended objects are also edited, or the effect is highly inconsistent across frames.

4 - The instruction is correctly and fully executed for the entire duration. Only minor attribute inaccuracies remain (e.g., slight colour or size mismatch, minor position offset). All and only the intended targets are affected.

5 - Perfect execution: every aspect of the instruction is faithfully reproduced - target, action, class, number, position, scale, pose, motion, style, and detail all exactly match the prompt throughout the entire video.

Dimension 2 Video Consistency

Evaluate whether non-edited regions and editing-irrelevant attributes remain consistent before and after editing. This includes: background preservation, art style / colour tone consistency, subject identity consistency, spatial layout and geometry preservation, and motion continuity.

Important: Changes that are a NECESSARY and EXPECTED consequence of the editing instruction itself should NOT be penalised (e.g., replacing the background naturally changes the background; changing material naturally alters texture). Only evaluate unintended or unnecessary deviations.

1 - The original scene is barely recognisable: background is completely destroyed, subject identity is lost, spatial layout is severely distorted, or art style is drastically and unnecessarily altered.

2 - The main subject is recognisable, but major unintended changes are present: background significantly altered without reason, subject's key features clearly different, or overall colour tone shifted noticeably.

3 - Overall structure and subject identity are maintained, but noticeable unintended deviations exist: moderate background changes, minor subject appearance drift, or mild art style inconsistency.

4 - Nearly all non-edited regions and attributes are well preserved. Only very minor, hard-to-spot deviations that do not affect the overall viewing experience. Motion is smooth and continuous.

5 - Perfect preservation: all non-edited regions, subject identity, background, art style, spatial layout, and motion are completely unchanged. The edit is perfectly isolated.

Dimension 3 Reference Image Consistency

Evaluate how well the edited result matches the reference image in terms of visual appearance. This is NOT a pixel-level comparison - it should be evaluated in the context of the editing instruction's intent. Focus on: Does the edited content capture the key visual characteristics of the reference image (shape, colour, texture, pattern, style, material, identity)? Is the resemblance faithful enough to recognise the reference as the source of inspiration?

Important: The reference image serves as a visual exemplar. The edit does not need to be a literal copy-paste - it should integrate the reference's visual characteristics naturally into the video scene while respecting the editing instruction's intent. A result that captures the essence (e.g., correct material/texture for a material change, correct object identity for a replacement, correct style for a style transfer) should score highly even if minor details differ.

1 - The edited content bears no resemblance to the reference image. The visual characteristics (shape, colour, texture, style, identity) are entirely different or absent.

2 - Very weak resemblance: only one or two superficial attributes vaguely match (e.g., similar general colour but wrong shape/texture/identity). The reference is not recognisable as the source.

3 - Moderate resemblance: the general category or style is correct, and some key visual features match, but significant differences remain in important attributes (e.g., correct object type but wrong colour/pattern, correct style direction but inconsistent execution).

4 - Strong resemblance: the edited content clearly reflects the reference image's key visual characteristics. Most attributes (shape, colour, texture, pattern, style, identity) are well captured. Only minor detail differences exist.

5 - Excellent match: the edited content faithfully reproduces the reference image's visual characteristics within the video context. All key attributes are accurately captured, and the integration feels natural and intentional.

Dimension 4 Generation Quality

Evaluate the visual quality, temporal stability, and physical plausibility of the edited video. Focus on: AI artifacts (pasting feel, unnatural blending, distortion, deformation), temporal coherence (flickering, jittering, "boiling" textures, frame discontinuity), seamlessness of integration (edges, colour/resolution matching, lighting/shadow consistency), and physical realism (correct perspective, shadows, reflections, occlusion, natural motion).

1 - Severe quality issues: extreme flickering or "boiling" effects, heavy distortion/deformation, obvious pasting feel with clear seams, or physically impossible results. The video is essentially unwatchable.

2 - Significant and distracting quality problems: obvious AI artifacts, strong temporal inconsistency, clear resolution/colour mismatch, or major physical implausibilities.

3 - Noticeable but tolerable issues: moderate AI feel, some flickering or texture instability, minor edge artefacts, or small physical inconsistencies. The video is watchable but the edit is clearly visible.

4 - Good quality with only minor issues: very slight AI artifacts visible only upon close inspection, largely stable, well-matched lighting and colour, and believable physical interactions.

5 - Flawless quality: perfectly stable and temporally coherent, completely seamless integration, physically correct throughout, and natural motion. The edit is indistinguishable from the original footage.

Dimension 5 Overall Performance

Provide a holistic assessment: considering all the above dimensions together, how well does the edited video meet the user's likely expectation? This score reflects overall subjective satisfaction - whether the result would be accepted by a real user as a successful reference-guided edit.

1 - Completely fails to meet user expectations. The edit is unusable.

2 - The edit attempt is recognisable but the result is clearly unacceptable due to combined failures across dimensions.

3 - A partially successful edit: the intent is understood and partially achieved, but noticeable issues in one or more dimensions reduce the result's usability.

4 - A good edit that would satisfy most users. Minor imperfections exist but do not significantly detract from the overall result.

5 - An excellent edit that fully meets or exceeds user expectations. The result is professional-grade, faithfully reflects the reference, and is virtually indistinguishable from a real or manually crafted video.

Scoring Constraints

- If the instruction is not executed at all (non-execution), Instruction Compliance should be scored 1, and Video Consistency, Reference Image Consistency, and Generation Quality should be skipped (marked as "N/A"). Overall Performance should be 1.

Response Format

Please output a valid JSON object exactly matching the following structure, without any extra markdown formatting or conversational text:

```
{  
  "Brief reasoning": "<A concise explanation covering all five dimensions, no more than 60 words.>",  
  "Instruction Compliance": "<1-5>",  
  "Video Consistency": "<1-5 or \"N/A\">",  
  "Reference Image Consistency": "<1-5 or \"N/A\">",  
  "Generation Quality": "<1-5 or \"N/A\">",
```

```
"Overall Performance": "<1-5>"
}}
```

editing instruction is: {edit_prompt}.

Below are the original video, reference image, and edited video:

Prompt 2. Bernini-RV2V evaluation prompt

B Experimental Results

B.1 More Qualitative Comparison with SoTA Methods



Figure 19 Qualitative Comparison with SoTAs on V2V task.

Figure 19 shows additional results on V2V tasks. In the case on the left, neither Wan-2.7 nor Kling-O3 follows the instruction to modify the white tiger’s motion. VINO changes the motion, but the standing tiger keeps its paw on the lying tiger throughout the video, making the action look unnatural. In contrast, Bernini correctly produces the “scratching” motion. For the middle case, which involves shifting the focus, only Bernini moves the focus to the girl in the background while blurring the foreground. In the case on the right, which involves changing the material, all models successfully modify the material, but only Bernini preserves the tea and tea leaves inside the teacup.

Figure 20 presents additional qualitative comparisons on the VR2V task. In the first case, both VINO and Kling alter the girl’s facial features, Wan-2.7 changes the overall lighting of the video, while Bernini correctly modifies only the girl’s hairstyle. In the middle case, which involves changing the background, only Bernini removes the snow on the ground beneath the person’s feet from the original video. In the case on the right, only Bernini accurately applies the style of the reference image while preserving the original shape of the tree.



Figure 20 Qualitative Comparison with SoTAs on RV2V task.

B.2 Qualitative Comparison of Video Editing with Reasoning

Figure 21 present qualitative comparisons across different reasoning variants. The visualization reveals that while the baseline struggles with complex layout adjustments and imaginary state changes, incorporating self-generated textual reasoning yields notable improvements in instruction following. Employing an LLM rewriter to refine input prompts further enhances performance, producing results with better structure and precision. The intermediate CoT images provide essential visual grounding, ensuring superior alignment for challenging scenarios such as out-of-distribution tasks.

B.3 More Generalization Results

Figure 22 presents additional generalization examples on diverse video editing instructions beyond those covered during training, including expression change, perspective change, spatial reasoning, temporal reasoning, effect addition, atmosphere rendering, subject interaction, and composed editing. Although these editing types are absent from the V2V training data, Bernini is still able to execute them effectively. These results indicate that Bernini develops a transferable instruction-following capability that extends beyond the specific editing patterns observed during training.



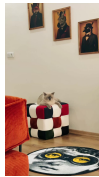





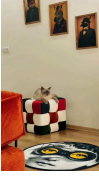
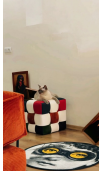






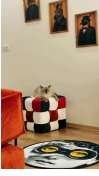
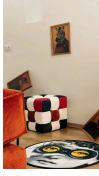






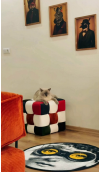
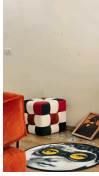







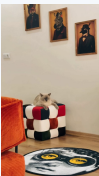


	Case 1	Case 2	Case 3	Case 4
Source Video (First Frame)	 <i>Prompt: Make the pizza appear evenly divided into six slices.</i>	 <i>Prompt: If the food is cooked over excessively high heat, what would it turn out like?</i>	 <i>Prompt: If a picture frame suddenly falls from the wall, how would the cat react?</i>	 <i>Prompt: Reposition the child to the man's left side.</i>
Direct Editing (No Reasoning)	<div style="display: flex; justify-content: space-around;"> <div>First Frame </div> <div>Last Frame </div> </div>	<div style="display: flex; justify-content: space-around;"> <div>First Frame </div> <div>Last Frame </div> </div>	<div style="display: flex; justify-content: space-around;"> <div>First Frame </div> <div>Last Frame </div> </div>	<div style="display: flex; justify-content: space-around;"> <div>First Frame </div> <div>Last Frame </div> </div>
Self-text (Text Reasoning)	<i>CoT Text:</i> Divide the pizza into six even slices... ensuring each slice is clearly separated. <div style="display: flex; justify-content: space-around;">   </div>	<i>CoT Text:</i> If the food is cooked over excessively high heat... it would likely turn out overcooked and dry. <div style="display: flex; justify-content: space-around;">   </div>	<i>CoT Text:</i> The cat would likely be startled... possibly running across the room to find a safe spot. <div style="display: flex; justify-content: space-around;">   </div>	<i>CoT Text:</i> Reposition the child to sit on the man's left side... The child should be holding the smartphone. <div style="display: flex; justify-content: space-around;">   </div>
PE (GPT-5.4) (Prompt rewrite)	 	 	 	 
Self-vision-text (Vision-text Reasoning)	<i>Step1: CoT Image</i>  ↓ <i>Step2: Generated Video</i> 	<i>Step1: CoT Image</i>  ↓ <i>Step2: Generated Video</i> 	<i>Step1: CoT Image</i>  ↓ <i>Step2: Generated Video</i> 	<i>Step1: CoT Image</i>  ↓ <i>Step2: Generated Video</i> 

Figure 21 Qualitative comparisons of different inference modes. For each video, we display the first and last frames. The methods are arranged from top to bottom, employing increasingly sophisticated reasoning patterns that lead to progressively improved editing quality. Our self-supervised vision-text reasoning further introduces a visual intermediate (the CoT image) to ground the process in the visual domain, yielding superior spatial fidelity and temporal consistency.

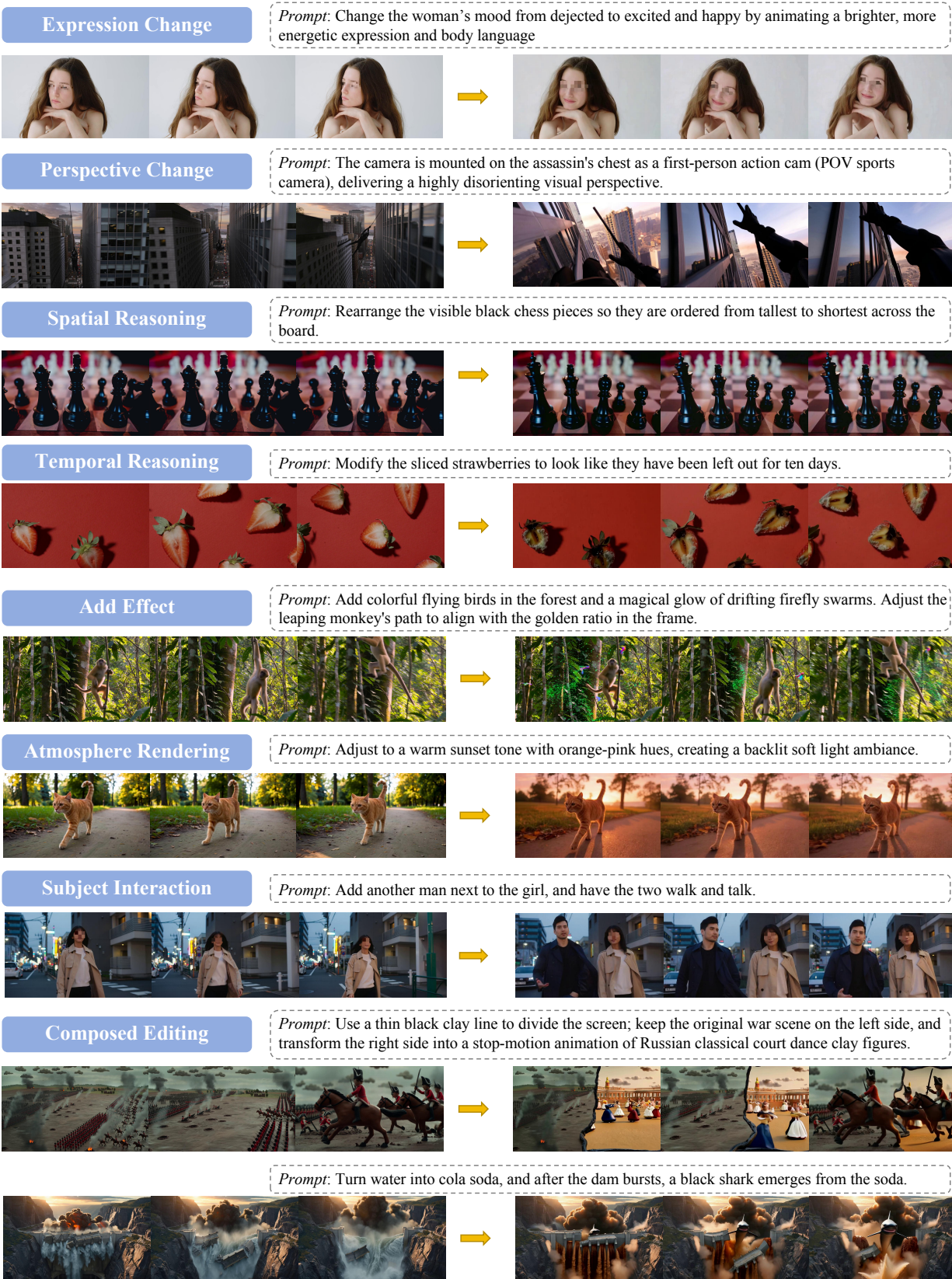


Figure 22 More generalization to diverse video editing instructions.